Reduced PaxillinB localization to cell-substrate adhesions promotes cell migration in *Dictyostelium*

Julio C. Fierro Morales[1], Chandler Redfearn[2], Margaret A. Titus[3] and Minna Roh-Johnson[1]

[1]Department of Biochemistry, University of Utah, Salt Lake City, UT, 84112, USA
[2]Department of Kinesiology, North Carolina Agricultural and Technical State University, Greensboro, NC 27411, USA
[3]Department of Genetics, Cell Biology, and Development, University of Minnesota, Minneapolis, MN 55455, USA

*Correspondence: roh-johnson@biochem.utah.edu

Abstract

Many cells adhere to extracellular matrix for efficient cell migration. This adhesion is mediated by focal adhesions, a protein complex linking the extracellular matrix to the intracellular cytoskeleton. Focal adhesions have been studied extensively in mesenchymal cells, but recent research in physiological contexts and amoeboid cells suggest focal adhesion regulation differs from the mesenchymal focal adhesion paradigm. We used *Dictyostelium discoideum* to uncover new mechanisms of focal adhesion regulation, as *Dictyostelium* are amoeboid cells that form focal adhesion-like structures for migration. We show that PaxillinB, the *Dictyostelium* homologue of Paxillin, localizes to dynamic focal adhesion-like structures during *Dictyostelium* migration. Unexpectedly, reduced PaxillinB recruitment to these structures increases *Dictyostelium* cell migration. Quantitative analysis of focal adhesion size and dynamics show that lack of PaxillinB recruitment to focal adhesions does not alter focal adhesion size, but rather increases focal adhesion turnover. These findings are in direct contrast to Paxillin function at focal adhesions during mesenchymal migration, challenging the established focal adhesion model.

Subjects: Adhesion, Cytoskeleton, Migration, Motility

Short Summary: Fierro Morales et al. show that the role of PaxillinB in focal adhesion-based migration differs from the canonical mesenchymal focal adhesion paradigm.

[1] Lead contact: roh-johnson@biochem.utah.edu

INTRODUCTION

Single cell migration is a pivotal aspect of several developmental, immunological and disease processes, with cells being able to switch between distinct forms of motility depending on the environmental context (De Pascalis and Etienne-Manneville, 2017; Merino-Casallo et al., 2022; Petrie and Yamada, 2016; Trepat et al., 2012). This ability to switch between different migration forms is important for cells to adapt to unique environments (De Pascalis and Etienne-Manneville, 2017; Pawluchin and Galic, 2022; Yamada and Sixt, 2019). Cell migration is often categorized into two overarching forms: amoeboid migration and mesenchymal migration, although cell migration should be considered as more of a spectrum of states (Kunwar et al., 2006; Te Boekhorst et al., 2016; Yamada and Sixt, 2019). Amoeboid motility, which is typically associated with immune cells such as neutrophils and T cells, is defined by low adhesion to the surrounding extracellular matrix (ECM), protrusion through pores in the extracellular matrix (ECM), and increased actomyosin contractility (Friedl and Wolf, 2010; Lammermann and Sixt, 2009; Pawluchin and Galic, 2022; Rodriguez-Hernandez et al., 2016; Schick and Raz, 2022; Yamada and Sixt, 2019). In contrast, mesenchymal migration is characterized by adhesion to the ECM, a rich actin network at the leading edge and proteolysis of the ECM, with cells such as fibroblasts, neural crest cells and several cancer cell lines using this form of motility (Kunwar et al., 2006; Merino-Casallo et al., 2022; Pawluchin and Galic, 2022; Yamada and Sixt, 2019).

Research focused on mesenchymal migration has shown that cells use adhesion structures called focal adhesions. Focal adhesions are multilayered nanostructures composed of hundreds of proteins that physically link the surrounding ECM to the intracellular actin cytoskeleton (Case and Waterman, 2015; Kanchanawong et al., 2010; Lo, 2006). The transmembrane proteins that physically link focal adhesions to the ECM are integrin heterodimers. Upon integrin interaction with the ECM, a series of mechanosensitive and biochemical signals regulate cycles of focal adhesion assembly and disassembly. This cycle in turn promotes efficient mesenchymal cell migration (referred to as adhesion-based migration going forward) (Geiger et al., 2009; Lock et al., 2008; Oakes and Gardel, 2014). There is extensive literature dissecting focal adhesions during adhesion-based migration, and the majority has focused on mesenchymal cells in flat, *in vitro* 2D systems (Fierro Morales et al., 2022). These studies have led to an established model of focal adhesion components, assembly, and dynamics characterized by large, mature focal adhesion structures that generate traction forces and a slower rate of migration compared to other forms of motility such as amoeboid migration (Case and Waterman, 2015; Gardel et al., 2010; Kanchanawong et al., 2010; Liu et al., 2015; Pankova et al., 2010; Parsons et al., 2010). Recent research dissecting focal adhesion formation and regulation in other contexts and cell types, however, has led to questions as to the criteria defining focal adhesions and the cells capable of making them.

Work on focal adhesions in physiological contexts has provided evidence of focal adhesion regulation that differs from the canonical mesenchymal paradigm. Previously, we showed that focal adhesions in migrating cells *in vivo* are smaller and more dynamic than *in vitro* adhesions, and regulation of a core focal adhesion component Paxillin is distinct than what is observed in mammalian *in vitro* systems (Xue et al., 2023). Additional work looking at "curved" focal adhesions in physiological conditions, meanwhile, has also called into question the localization of core components such as FAK and Vinculin to focal adhesions (Zhang et al., 2023). Intriguingly,

these focal adhesion characteristics are similar to those observed in recent work characterizing focal adhesions in non-mesenchymal cells. In contrast to mesenchymal cells, amoeboid cells such as T cells and neutrophils use a fast-moving motility characterized by a round cell shape and an independence from integrin-mediated focal adhesions to navigate their environment (Friedl et al., 2001; Friedl et al., 1998; Lammermann et al., 2008; Lammermann and Sixt, 2009; Paluch et al., 2016; Pinner and Sahai, 2009). Interestingly, studies suggest neutrophils still generate traction forces during migration and require integrin to migrate through stiff substrates (Jannat et al., 2010; Oakes et al., 2009; Paysan-Lafosse et al., 2023; Shin et al., 2010; Smith et al., 2007), though studies visualizing putative focal adhesions are lacking. Similarly, T cells generate traction forces by adhering to the surrounding ECM and this process is integrin-dependent, suggestive of adhesion-based migration, although there had been no reports of directly visualizing focal adhesions in T-cells (Du et al., 2016; Fernandes et al., 2020; Gaylo-Moynihan et al., 2019; Overstreet et al., 2013). However, recently, work has shown that when T cells are confined in conditions mimicking the physiological environment, T-cells make focal adhesions containing core components such as Integrin, Talin, and Vinculin (Caillier et al., 2023). Notably, these focal adhesions are smaller, more dynamic, and generate reduced traction forces compared to focal adhesions made by canonical mesenchymal cells (Caillier et al., 2023). Altogether, these studies have challenged aspects of the canonical model of focal adhesions as well as the cell types and contexts in which they are thought to be capable of being formed. This current body of work suggests that further studies into the regulation and composition of focal adhesions in non-mesenchymal contexts are necessary to paint a more holistic picture of how focal adhesions are utilized and regulated by different cells in different contexts.

One context of particular interest for investigating previously undiscovered forms of focal adhesion regulation is in evolutionarily distant species. Classically, focal-adhesion based migration has been considered unique to Metazoans while amoeboid motility is found across Eukaryotes (Brunet et al., 2021; Devreotes and Zigmond, 1988; Fritz-Laylin et al., 2017; Fritz-Laylin and Titus, 2023; Velle and Fritz-Laylin, 2019; Velle and Fritz-Laylin, 2020). Interestingly, while the focal adhesion machinery itself was originally believed to be a Metazoan-specific innovation, genomic analysis of non-Metazoan organisms identified putative homologues of various core components of focal adhesions in organisms as evolutionarily distant as Amoebozoa, suggesting that this machinery originated prior to the divergence of Metazoa (Fierro Morales et al., 2022; Hynes and Zhao, 2000; Rokas, 2008; Sebe-Pedros et al., 2010). Furthermore, focal adhesion homologues are present in non-Metazoan species that are believed to predominantly use focal adhesion-independent migration (ie. amoeboid-like migration). This seemingly paradoxical finding raises questions regarding if and how these organisms use focal adhesions for cell migration, and whether the regulation is similar to that observed in mammalian systems. Among these non-Metazoan species possessing focal adhesion machinery is the model Amoebozoan, *Dictyostelium discoideum*. Studies investigating focal adhesion-like structures in *Dictyostelium* suggest these amoebae are capable of forming actin-rich adhesion structures that contain homologues of several focal adhesion proteins (Berman et al., 2000; Bukharova et al., 2005; Cornillon et al., 2008; Cornillon et al., 2006; Cornillon et al., 2000; Duran et al., 2009; Fey et al., 2002; Froquet et al., 2012; Hibi et al., 2004; Nagasaki et al., 2009; Niewohner et al., 1997; Patel et al., 2008; Plak et al., 2016; Pribic et al., 2011; Tsujioka et al., 2004; Tsujioka et al., 2008), and generate traction forces on the substratum during migration, reminiscent of focal adhesions (Copos et al., 2017; Iwadate and Yumura, 2008a; Mijanovic and Weber, 2022; Uchida and Yumura, 2004).

Interestingly, homology analyses of core focal adhesion components suggest *Dictyostelium* possess putative homologues of some but not all components (Fierro Morales et al., 2022; Sebe-Pedros et al., 2010), indicating that *Dictyostelium* is able to use focal adhesion-based migration despite lacking core components thought to be pivotal for proper focal adhesion formation and function.

Though this body of research indicates *Dictyostelium* forms focal adhesions for efficient migration – much like in mesenchymal cells – *Dictyostelium* single cell migration is associated with amoeboid migration and often used as a comparative model for other amoeboid cells such as leukocytes (Devreotes and Zigmond, 1988; Friedl et al., 2001; Fukui and Inoue, 1997; Paluch et al., 2016). Studies showing that other amoeboid cells such as T cells are capable of forming focal adhesions that differ from the canonical mesenchymal paradigm (Caillier et al., 2023; Overstreet et al., 2013), however, beg the question of whether *Dictyostelium* is also forming focal adhesions that differ from classic focal adhesions. The work demonstrating *Dictyostelium's* use of homologues of core focal adhesion components for adhesion-based migration, in conjunction with its amoeboid migration-like characteristics, make it an ideal system for investigating novel aspects of focal adhesion function and regulation during cell migration in non-mesenchymal contexts such as amoeboid cells. Furthermore, the lack of putative homologues of certain core focal adhesion components makes *Dictyostelium* an interesting model to investigate how focal adhesions are assembled and regulated for efficient migration in conditions where key components are missing, as this can give insight into differential modes of focal adhesion regulation and assembly relevant to physiological environments (Caillier et al., 2023; Xue et al., 2023; Zhang et al., 2023).

We sought to understand how *Dictyostelium* form and regulate focal adhesions during single cell migration. We focused on characterizing PaxillinB, the *Dictyostelium* homologue of the focal adhesion scaffolding molecule Paxillin. We dissected the functions of PaxillinB at *Dictyostelium* focal adhesions and identified key conserved domains required for PaxillinB localization and stability at focal adhesions. Unexpectedly, however, we found that reduced PaxillinB recruitment to focal adhesions *increased Dictyostelium* cell migration velocity. This increase in cell migration velocity was not due to a switch to an adhesion-independent form of migration, but rather, an increased rate of focal adhesion turnover. These findings are in contrast to Paxillin regulation in mammalian cells, and suggest that focal adhesion regulation differs in organisms capable of undergoing amoeboid migration. These results further challenge the canonical model of focal adhesion regulation during cell migration.

RESULTS

Dictyostelium discoideum possesses putative homologues of key focal adhesion components

To investigate mechanisms of focal adhesion formation, function, and regulation in *Dictyostelium*, we first sought to identify which focal adhesion components (as defined by mammalian systems) are present in *Dictyostelium*. While work using BLASTp to look at sequence conservation identified putative homologues of core focal adhesion components in *Dictyostelium* (Sebe-Pedros et al., 2010), incorporating novel domain architecture-based and structural-based homology tools can provide higher sensitivity for homologue detection, particularly for distantly evolutionarily-related proteins (Illergard et al., 2009; Lee and Lee, 2009; Potter et al., 2018; van Kempen et al.,

2023). Thus, we used a combination of bidirectional homology queries using BLASTp (McGinnis and Madden, 2004), PHMMR (Potter et al., 2018), and FoldSeek (van Kempen et al., 2023) to test for sequence, domain architecture, and predicted structural homology, respectively.

Consistent with previous studies, our analyses suggest that homologues of some core focal adhesions molecules (Sebe-Pedros et al., 2010), particularly those involved in scaffolding and force transduction, originated in Eukaryotes, just prior to the divergence of Amoebozoans **(Figure S1A and S1B).** Homologues of other proteins necessary for mammalian focal adhesion formation – such as the tyrosine kinases and integrins – appear to have evolved separately. We also sought to identify specific non-Metazoan organisms that have been shown to form cell-substrate structures through functional analyses and/or imaging-based studies **(Figure S1A).** We found that these organisms, including *Dictyostelium*, possess homologues of some but not all core focal adhesion molecules **(Figure S1A).** Specifically, *Dictyostelium* lacks putative homologues of the key tyrosine kinases focal adhesion kinase (FAK) and c-SRC **(Figures 1A and S1A).** Furthermore, *Dictyostelium* possesses the SIB (Similar to Integrin Beta) molecules, which are potential putative beta integrin-like proteins composed of a mix of conserved beta integrin domains and bacterial adhesion domains (Cornillon et al., 2008; Cornillon et al., 2006). While SIBs are hypothesized to be serve as beta-integrin-like adhesion receptors, to the best of our knowledge no work has been done to confirm this function. These homology results, combined with previous work demonstrating formation of focal-adhesion like structures in *Dictyostelium* (Berman et al., 2000; Bukharova et al., 2005; Cornillon et al., 2008; Cornillon et al., 2006; Cornillon et al., 2000; Duran et al., 2009; Fey et al., 2002; Froquet et al., 2012; Hibi et al., 2004; Nagasaki et al., 2009; Niewohner et al., 1997; Patel et al., 2008; Plak et al., 2016; Pribic et al., 2011; Tsujioka et al., 2004; Tsujioka et al., 2008), suggest that *Dictyostelium* are capable of forming focal adhesions without possessing all the components necessary for mammalian focal adhesion formation. We therefore next determined the mechanism of focal adhesion formation (herein referred to as cell-substrate adhesions) in this amoeba.

The *Dictyostelium* Paxillin homologue localizes to cell-substrate adhesions at the ventral surface

Of the focal adhesion homologues present in *Dictyostelium*, one protein of particular interest was PaxillinB, the *Dictyostelium* homologue of the scaffolding molecule Paxillin. In mammalian systems, Paxillin is a key scaffolding protein involved in regulating focal adhesion dynamics and cell migration via interactions with other focal adhesion components such as FAK, c-SRC, Vinculin, CRKII and others (Lopez-Colome et al., 2017; Schaller and Parsons, 1995; Turner et al., 1990). Initial work using PaxillinB overexpression in *Dictyostelium* suggests that PaxillinB localizes to bright ventral surface foci (Bukharova et al., 2005; Nagasaki et al., 2009; Patel et al., 2008; Pribic et al., 2011) reminiscent of cell-substrate adhesions (Beningo et al., 2001; Hu et al., 2014; Xue et al., 2023). Furthermore, knockout of PaxillinB decreased cell adhesion in response to shaking (Bukharova et al., 2005; Nagasaki et al., 2009), suggesting that PaxillinB function is involved in cell adhesion to the underlying substrate. However, how or whether PaxillinB regulates cell-substrate adhesion dynamics during *Dictyostelium* cell migration is unclear. Additionally, *Dictyostelium* lacks putative homologues for FAK and cSRC – which form a cognate binding axis with Paxillin to regulate adhesion dynamics in mammalian systems (Bellis et al., 1997; Burridge et al., 1992; Mitra et al., 2005; Sachdev et al., 2009; Schaller and Schaefer, 2001) – suggesting a

232 unique and potentially novel mechanism for Paxillin regulation. Thus, we investigated the role of
233 PaxillinB at *Dictyostelium* cell-substrate adhesions during migration.
234
235 Using a *paxb-* line that has endogenous PaxillinB knocked out, we first sought to determine
236 whether PaxillinB regulates cell spreading – often used as an indicator of cell adhesive capability.
237 We found that knockout of PaxillinB led to a defect in cell spreading **(Figure 1B)**, suggesting
238 reduced cell adhesive capacity with the underlying substrate**.** We tested cell-substrate adhesion
239 formation more directly by next determining whether PaxillinB localizes to punctate structures at
240 the cell ventral surface, in line with focal adhesions observed in mammalian cells. Previous
241 research examining PaxillinB ovexpression in a *paxb-* background suggests overexpression does
242 not perturb PaxillinB function (Bukharova et al., 2005), so we overexpressed GFP-tagged
243 PaxillinB under an actin15 promoter in a *paxb-* background to visualize PaxillinB at the cell ventral
244 surface. Imaging of fluorescently-tagged PaxillinB using spinning disc confocal microscopy in the
245 *paxb-* background showed localization of PaxillinB to ventral surface foci **(Figure 1C and Video**
246 **S1),** in line with previous imaging studies (Bukharova et al., 2005; Nagasaki et al., 2009; Patel et
247 al., 2008; Pribic et al., 2011). Additional imaging using total internal reflection fluorescence
248 (TIRF) microscopy confirmed PaxillinB localizes to ventral surface foci **(Figure S2 and Video**
249 **S2)**. Consistent with these structures being cell-substrate adhesion, these PaxillinB positive foci
250 co-localized with actin, marked by RFP:Lifeact, at dynamic structures at the leading edge of the
251 cell **(Figure 1C and Video S1).** Furthermore, perturbation of actin polymerization via
252 LatrunculinA spike-in, which is commonly used to perturb cell-substrate adhesions (Cai et al.,
253 2000), led to ablation of PaxillinB punctae shortly after spike-in **(Figure 1D and Video S3),**
254 suggesting PaxillinB localization is actin-dependent. We also tested co-localization of PaxillinB
255 with other *Dictyostelium* cell-substrate adhesion component homologues. Knockout of the two
256 *Dictyostelium* Talin homologues, TalinA and TalinB, has been shown to perturb PaxillinB
257 localization (Tsujioka et al., 2008). Therefore, we examined co-localization of PaxillinB with Talin
258 molecules and found that PaxillinB co-localized with TalinB at ventral surface foci at the leading
259 edge **(Figure 1E and Video S4)**. Altogether, these data suggest PaxillinB localizes to dynamic
260 cell-substrate adhesions in *Dictyostelium*.
261
262 Focal adhesion size regulates adhesion-based migration, in which increased focal adhesion size
263 correlates with increased migration speed until the adhesion size reaches a threshold at which point
264 speed decreases (Kim and Wirtz, 2013). Thus, we next sought to quantify the size as well as the
265 number of PaxillinB-positive cell substrate adhesions. We developed a semi-automated image
266 processing pipeline on ImageJ to quantify single timepoint images of individual cells expressing
267 GFP:PaxillinB. This pipeline allows us to increase the signal-to-noise ratio, and identify and
268 quantify individual PaxillinB punctae in an unbiased manner **(Figures 1F and 1G).** Using this
269 tool, we observed a wide range of Paxillin punctae numbers per cell ranging from one to 23, with
270 an average area of ~0.096 microns^2 **(Figure 1H).** The average size of the PaxillinB-positive
271 punctae is much smaller than previously described size criteria for focal adhesions in mesenchymal
272 Metazoan systems, which are typically 0.6 microns^2 (Gardel et al., 2010; Han et al., 2021; Han et
273 al., 2015). Indeed, PaxillinB punctae size is more reminiscent of focal adhesions visualized in
274 physiological contexts (~0.1-0.2 microns^2 for "curved" adhesions (Zhang et al., 2023) and ~0.3
275 microns^2 for zebrafish melanoma cells *in vivo* (Xue et al., 2023)) as well as nascent focal contacts
276 in mammalian cells (0.24 microns^2) (Han et al., 2021; Han et al., 2015). Together these data
277 suggest *Dictyostelium* is an amoeboid cell capable of forming PaxillinB-positive focal adhesion-

like structures, and we next sought to determine how PaxillinB regulates these structures during cell migration.

C-terminal LIM domains are required for PaxillinB localization

Our works shows that PaxillinB localizes to cell-substrate adhesions in *Dictyostelium*, consistent with previous work (Bukharova et al., 2005; Nagasaki et al., 2009; Patel et al., 2008; Pribic et al., 2011). We next determined which domains are required for PaxillinB localization and function at cell-substrate adhesions. Previous work (Bukharova et al., 2005) using pairwise sequence alignments of *Dictyostelium* and human Paxillin molecules suggest conservation of N-terminal leucine-rich LD motifs and C-terminal LIM (**L**in-11, **I**sl-1 and **M**ec-3) domains, but not of the Tyrosine 31 (Y31) and Tyrosine 118 (Y118) residues that are phosphorylated by upstream kinases, FAK and c-SRC (Bellis et al., 1997; Burridge et al., 1992; Mitra et al., 2005; Sachdev et al., 2009; Schaller and Schaefer, 2001). We sought to build on this work by using multiple sequence alignments of Paxillin molecules from various organisms to identify Paxillin features that are conserved across evolutionary space and likely to be fundamental aspects of cell-substrate adhesion function and regulation as opposed to just similarities between *Dictyostelium* and human Paxillin molecules. Furthermore, we used domain architecture and predicted structural homology tools (McGinnis and Madden, 2004; Potter et al., 2018; van Kempen et al., 2023) utilized for our bidirectional homology pipeline **(Figure S1)** to provide higher sensitivity during comparative analyses.

Comparisons of the structure, domain, and sequence architecture of Paxillin molecules across several organisms shows conservation across the N-terminal LD motifs, and C-terminal LIM domains **(Figure 2A).** Quantitative homology analyses between human and *Dictyostelium* Paxillin molecules showed a higher degree of structural and sequence similarity between the C-terminal LIM domains of the two proteins versus the N-termini and the proteins as a whole **(Figure 2B).** On the N-terminus, while vertebrate Paxillin proteins possess five LD motifs, which are binding sites of other focal adhesion proteins (Lopez-Colome et al., 2017), non-vertebrate Paxillin molecules possess varying numbers of LD motifs including four motifs in *Dictyostelium* PaxillinB **(Figure 2A)**. The sequences surrounding the LD motifs, however, are not well-conserved. Thus, we examined these specific motifs closer, focusing on residues important for the FAK-Paxillin interaction axis in mammalian systems. Using multiple sequence alignments, we observed Paxillin Y31 and Y118 residues are limited to Vertebrate and Metazoan Paxillin molecules, respectively, as none of the Amoebozoan Paxillin proteins including *Dictyostelium* PaxillinB possessed these residues **(Figure 2C),** consistent with previous work (Bukharova et al., 2005)**.** We also used multiple sequence alignments to evaluate conservation of key aspartic acid and arginine residues in the LD2 motif necessary for FAK binding to Paxillin molecules (Brown et al., 1996). While the aspartic acid residue was well conserved, the arginine residue was only found in vertebrate Paxillin proteins and was not substituted with another basic amino acid **(Figure 2D).** These data suggest the FAK-Paxillin binding axis and phosphorylation activity is likely not conserved in *Dictyostelium* PaxillinB. Furthermore, these observations suggest the Paxillin-FAK binding axis-based regulation of cell-substrate adhesions seen in mammalian systems likely occurs through some other mechanism in *Dictyostelium*, if at all.

We next focused on the conserved C-terminal LIM domains and residues involved in focal adhesion functions **(Figure 2B).** We performed phylogenetic analyses of the LIM domains of

Paxillin proteins across Eukaryotic species, along with the LIM domains of other LIM domain-containing proteins. These analyses showed that the LIM domains of Amoebozoan Paxillin molecules, including *Dictyostelium* PaxillinB, cluster with other Paxillin molecules **(Figure S3A)** as well as Leupaxin, a vertebrate specific member of the Paxillin superfamily. These data suggest *Dictyostelium* PaxillinB LIM domains are evolutionarily similar to the LIM domains of other Paxillin molecules. Previous functional analyses of Paxillin LIM domains suggest the LIM3 domain, specifically two zinc-coordinating cysteine residues found in a zinc-finger motif in the domain, is necessary for localization of Paxillin to focal adhesions (Brown et al., 1996). Multiple sequence alignments of only the LIM3 domain of Paxillin proteins suggest these cysteine residues are well conserved across species, with Amoebozoan Paxillin molecules – including *Dictyostelium* PaxillinB – possessing an acceptable histidine substitution (Cassandri et al., 2017) at one of these residues **(Figure 2E)**. A closer look at this histidine residue in the Alphafold predicted structure of *Dictyostelium* PaxillinB suggests the zinc-coordinating pocket is conserved relative to the predicted human Paxillin structure **(Figure S3B).** Altogether, these data show *Dictyostelium* PaxillinB conservation of the C-terminal LIM domains and the residues involved in localization to cell-substrate adhesions, but not the N-terminal residues involved in FAK binding and phosphorylation **(Figure 2F).** Furthermore, it suggests a mechanism for Paxillin localization to cell-substrate adhesions that we next tested.

Perturbation of PaxillinB LIM Domains Inhibits Localization to Cell-Substrate Adhesions and Increases Cell Migration

The Paxillin LIM3 domain has previously been shown to be required for Paxillin localization to focal adhesions in mammalian models (Brown et al., 1996). Due to the conservation of the LIM3 domain in *Dictyostelium* PaxillinB at the sequence and predicted protein folding level, we next tested for functional homology of this domain. We generated cells in which truncated GFP-tagged PaxillinB molecules, as well as RFP-tagged Lifeact to visualize actin, were expressed in the *paxb*-background **(Figure 3A)**. *Dictyostelium* expressing either wild-type PaxillinB (GFP:PaxB-WT) or a truncated PaxillinB only lacking the LIM4 domain, but still had the LIM3 domain (GFP:PaxB-ΔL4), showed PaxillinB punctae formation at the ventral surface of cells **(Figure 3B)**. These PaxillinB-positive punctae colocalized with actin at cell-substrate adhesions **(Figure 3B,** yellow arrowheads). Conversely, full truncation of all LIM domains (GFP:PaxB-ΔLIMS) led to full disruption of PaxillinB punctae formation, although still appeared to form actin-rich foci **(Figure 3B,** white arrowheads**).** To our surprise, however, cells expressing truncated PaxillinB proteins that lacked the LIM3 domain, but had at least one other LIM domain (GFP:PaxB-ΔL3, GFP:PaxB-ΔL34 and GFP:PaxB-ΔL234), still showed PaxillinB punctae formation and co-localization with actin **(Figure 3B)**, suggesting that PaxillinB was still able to localize to cell-substrate adhesions despite LIM3 domain perturbation.

We next asked how disrupting Paxillin LIM domains affected cell-substrate adhesion formation. We quantified the number of PaxillinB-positive cell substrate adhesions in the LIM mutants. Quantification of PaxillinB-positive punctae revealed that perturbation of the LIM3 domain, either by itself or in conjunction with the truncation of other LIM domains, led to a significant decrease in the average number of PaxillinB punctae formed per cell **(Figure 4A).** Interestingly, while the number of PaxillinB punctae was affected, there was no significant impact on size of the punctae that did form **(Figure S4A).**

370 We then investigated whether disrupting the PaxillinB LIM domains had an effect on cell
371 migration by quantifying *Dictyostelium* cell migration velocities and mean square displacement,
372 which is a measure of persistence (Gorelik and Gautreau, 2014). Surprisingly, cells expressing
373 truncated PaxillinB proteins demonstrated increased average cell velocity and mean square
374 displacement relative to those expressing wildtype PaxillinB **(Figures 4B and 4C).** Interestingly,
375 the trend in average cell migration velocity and mean square displacement is inversely correlated
376 with the number of PaxillinB punctae, with *increased* cell migratory ability correlating with a
377 *decreased* number of PaxillinB-positive cell-substrate adhesions. These results led us to
378 hypothesize that either reduced PaxillinB localization to cell-substrate adhesion altered adhesion
379 dynamics increasing cell migration rates; or that reduced PaxillinB localization to cell-substrate
380 adhesions transitioned cells to an adhesion-independent form of cell migration with increased
381 migration velocities.
382
383 To test between these hypotheses, we first determined whether disruption of PaxillinB cell-
384 substrate adhesion localization triggers a transition from an adhesion-based form of migration to
385 an adhesion-independent amoeboid motility, which is often associated with faster migration
386 velocity (Alexandrova et al., 2020; Pankova et al., 2010). A hallmark of amoeboid migration is
387 increased cortical contractility and accumulation of actin at the rear end of the polarized cell
388 (Alexandrova et al., 2020; Callan-Jones and Voituriez, 2016). Thus, we quantified the ratio of actin
389 density at the rear versus the front of migrating cells. Quantification of this ratio showed no
390 significant enrichment of actin at the rear versus the front of *Dictyostelium* cells expressing
391 truncated PaxillinB compared to those expressing wildtype PaxillinB **(Figure S4B)**. Furthermore,
392 as we show in Figure 1, timelapse imaging of *Dictyostelium* expressing GFP-PaxB shows
393 colocalization of PaxillinB foci with actin (**Figure S4C**, yellow arrowheads**)**. However, cells
394 expressing GFP:PaxB-ΔLIMS still show formation of actin-rich foci forming at the leading edge
395 of migrating cells despite not forming PaxillinB-positive punctae **(Figure S4D;** white
396 arrowheads**)**. Altogether, these results suggest that in the absence of PaxillinB localization,
397 *Dictyostelium* cells are still capable of forming cell-substrate adhesions and migrating used
398 adhesion-based motility.
399
400 The above results suggest that cell-substrate adhesions still form in the absence of PaxillinB
401 localization to these structures. Thus, we hypothesize that altered cell-substrate adhesion dynamics
402 may lead to the increased cell migration velocities observed in PaxillinB LIM domain mutants.
403 Using a semi-automated binary tracking pipeline on NIS-Elements AR (see Methods) to identify
404 PaxillinB punctae and track their duration across timelapse imaging videos, we quantified the
405 duration of PaxillinB punctae in *Dictyostelium* cells expressing either wildtype PaxillinB
406 (GFP:PaxB-WT) or truncated PaxillinB lacking the third and fourth LIM domains (GFP:PaxB-
407 ΔL34). The GFP:PaxB-ΔL34 line was chosen as it had a significant perturbation of PaxillinB
408 localization and increased cell migration but had a high enough number of PaxillinB punctae to
409 compare to wildtype PaxillinB punctae. Interestingly, we observed a significant reduction in
410 PaxillinB punctae duration in cells expressing GFP:PaxB-ΔL34 compared to cells expressing
411 GFP:PaxB-WT **(Figure 4D)**, suggesting faster turnover of these structures. Taken altogether, we
412 propose a model where perturbation of PaxillinB through LIM domain truncation leads to
413 decreased PaxillinB recruitment to cell-substrate adhesions. Reduced PaxillinB localization to cell
414 substrate adhesions then leads to increased adhesion turnover, resulting in increased cell migration
415 capability **(Figure 5).**

DISCUSSION

Though studies in 2D mesenchymal cell systems have led to an established model of focal adhesion composition, regulation and function, work characterizing focal adhesion structures in more physiologically relevant contexts and other cell types have shed light on novel compositions and characteristics of focal adhesions (Caillier et al., 2023; Xue et al., 2023; Zhang et al., 2023). These findings challenge the canonical framing of how focal adhesions are formed and which cells utilize them for efficient migration. This work led us to investigate how focal adhesions are formed and regulated for cell migration in different contexts. In this study, we characterize cell-substrate adhesions in *Dictyostelium discoideum*. *Dictyostelium* is classically considered as a model for amoeboid migration (Devreotes and Zigmond, 1988; Friedl et al., 2001; Fukui and Inoue, 1997; Paluch et al., 2016). However, the presence of focal adhesion homologues and formation of cell-substrate adhesions (Berman et al., 2000; Bukharova et al., 2005; Cornillon et al., 2008; Cornillon et al., 2006; Cornillon et al., 2000; Duran et al., 2009; Fey et al., 2002; Froquet et al., 2012; Hibi et al., 2004; Nagasaki et al., 2009; Niewohner et al., 1997; Patel et al., 2008; Plak et al., 2016; Pribic et al., 2011; Tsujioka et al., 2004; Tsujioka et al., 2008), make *Dictyostelium* an intriguing model system for investigating the regulation of cell-substrate adhesions. We focused on PaxillinB, the *Dictyostelium* homologue of Paxillin, and found it localized to small, dynamic cell-substrate adhesions at the ventral surface during cell migration. PaxillinB possesses conserved C-terminal LIM domains but not N-terminal features associated with the Paxillin-FAK binding axis. Perturbation of the LIM domains showed decreased PaxillinB localization to cell-substrate adhesions. Surprisingly, this perturbation led to an increase in cell migration velocity. Further analysis of punctae dynamics suggest LIM domain perturbation impacted the duration of cell substrate adhesions, which still form even after PaxillinB perturbation. These results suggest increased turnover of Paxillin at cell-substrate adhesions leads to increased cell migration **(Figure 5)**. Furthermore, these results provide evidence that amoeboid cells such as *Dictyostelium* utilize cell-substrate adhesions for cell migration and these cell-substrate adhesions have different composition and regulatory mechanisms than those seen in the traditional focal adhesion paradigm. This study adds to a growing field of work challenging the classic paradigm of focal adhesion function, assembly, and regulation for efficient migration.

One particularly surprising finding in our study is that perturbation of PaxillinB increases *Dictyostelium* cell migration velocity and persistence. Our data suggest perturbation of PaxillinB LIM domains leads to decreased PaxillinB localization, increased turnover of PaxillinB positive cell-substrate adhesions and increased migration speed **(Figure 4).** In mammalian systems, Paxillin functions as a key scaffold and regulatory hub at focal adhesions due to its interactions with several proteins. In *Dictyostelium*, we speculate that PaxillinB similarly serves as a scaffold, interacting with other proteins to regulate the stability and turnover of *Dictyostelium* cell-substrate adhesions. To investigate this hypothesis, future work is required to identify the interaction partners of PaxillinB at cell-substrate adhesions. While truncation of the LIM domains perturbs PaxillinB localization, it is unclear how the lack of PaxillinB localization regulates the localization and stability of other cell-substrate adhesion proteins. Other focal adhesion component homologues have been implicated in *Dictyostelium* cell-substrate adhesion function and cell migration (Bukharova et al., 2005; Cornillon et al., 2008; Cornillon et al., 2006; Fey et al., 2002; Froquet et al., 2012; Nagasaki et al., 2009; Niewohner et al., 1997; Tsujioka et al., 2008), however it is unclear if these proteins directly interact with PaxillinB or other components to regulate cell-

substrate adhesions. Further investigation into PaxillinB interactions at *Dictyostelium* cell-substrate adhesions via techniques such as unbiased protein-protein interaction screening will provide insight into novel aspects of cell-substrate adhesion regulation and composition in the context of an amoeboid cell.

Interestingly, *Dictyostelium* cell-substrate adhesions also appear to be similar to cell-substrate adhesions made by another cell type typically associated with amoeboid motility: T cells. Recent work showed T cells make focal adhesions that are smaller, more dynamic, and generate less traction forces compared to those made by traditional mesenchymal cells such as fibroblasts (Caillier et al., 2023). While we do not measure traction forces of the cell-substrate adhesions formed by *Dictyostelium,* the short-lasting nature of T-cell cell-substrate adhesions under confinement (~90 sec) is akin to the dynamic nature of *Dictyostelium* cell-substrate adhesions. These results suggest that amoeboid cells are likely forming more dynamic cell-substrate adhesions than mesenchymal cells, leading to a faster migration speed. This finding is consistent with our data showing that increased cell-substrate adhesion turnover in *Dictyostelium* correlates with faster migration speeds **(Figure 4D).** Intriguingly, both T cells (Caillier et al., 2023) and *Dictyostelium* (Iwadate and Yumura, 2008b) lack stress fibers; a lack of stress fibers has been previously associated with reduced recruitment of certain core adhesion molecules and adhesion maturation (Choi et al., 2008; Oakes et al., 2012). Of note, this phenomenon of reduced core component recruitment and adhesion maturation is also observed in cell-substrate adhesions formed in physiological contexts. Analysis of "curved" focal adhesions necessary for efficient migration in physiological contexts shows a lack of FAK and Vinculin recruitment to these adhesion sites (Zhang et al., 2023). Additionally, previous work from our lab examining focal adhesions of zebrafish melanoma cells *in vivo* indicate that zebrafish melanoma cells exhibit reduced levels of FAK and lack of Paxillin phosphorylation by FAK (Xue et al., 2023). Furthermore, preventing Paxillin phosphorylation promotes focal adhesion disassembly rates and single cell migration in vivo. These data are in stark contrast to focal adhesion regulation observed in mesenchymal cells *in vitro* and more akin to the cell-substrate adhesions we observe in *Dictyostelium*. Altogether, these data provide evidence of dynamic cell-substrate adhesions seen in amoeboid migration and physiological contexts that are different in composition, function, and regulatory mechanisms relative to the canonical focal adhesion model, challenging this traditional focal adhesion paradigm.

Dictyostelium's combination of a partially conserved focal adhesion toolkit and its amoeboid migration-like features make it an excellent model system to continue investigating cell-substrate adhesions that challenge our current framing of focal adhesions. Further characterization of *Dictyostelium* cell-substrate adhesions and their role in cell migration is an exciting avenue of research that will continue to shed light on novel forms of cell-substrate adhesion function and regulation. These findings can then be investigated in other cell types and physiologically relevant contexts. This investigation is important to re-define the criteria we use for focal adhesion formation and function during cell migration across various cell types and contexts.

Acknowledgments
We would like to thank all members of the Roh-Johnson lab for discussions and edits during manuscript preparation; Pascale Charest and the *Dictyostelium* Stock Center for *Dictyostelium* reagents; Nathan Roy and Carole Parent for helpful discussions about *Dictyostelium*; Lillian Fritz-

Laylin, Nathan Clark, Nels Elde, and Ellen Leffler for helpful discussion regarding phylogeny and organism choice; and the Cell Imaging Core at the University of Utah for use of Leica Yokogawa CSU-W1 spinning disc confocal microscope, Leica TCS SP8 laser confocal microscope, Nikon Yokogawa CSU-W1 spinning disc confocal microscope, and Nikon Gataca Systems Ilas2 TIRF platform and thank Michael Bridge and Xiang Wang for their assistance.

The work was funded by National Institutes of Health grant R00CA190836 (to M. Roh-Johnson) and National Institute of Allergy and Infectious Diseases grant # 01-00976-5000-59205460 (to BRIDGE UP-HBCU University of Utah)

Author contributions

Conceptualization, JCFM, MRJ; Methodology, JCFM, MAT, MRJ; Investigation, JCFM, CR, MAT; Formal Analysis, JCFM, CR; Writing, JCFM, MRJ; Funding acquisition, MRJ.

Competing interests

The authors declare no competing interests.

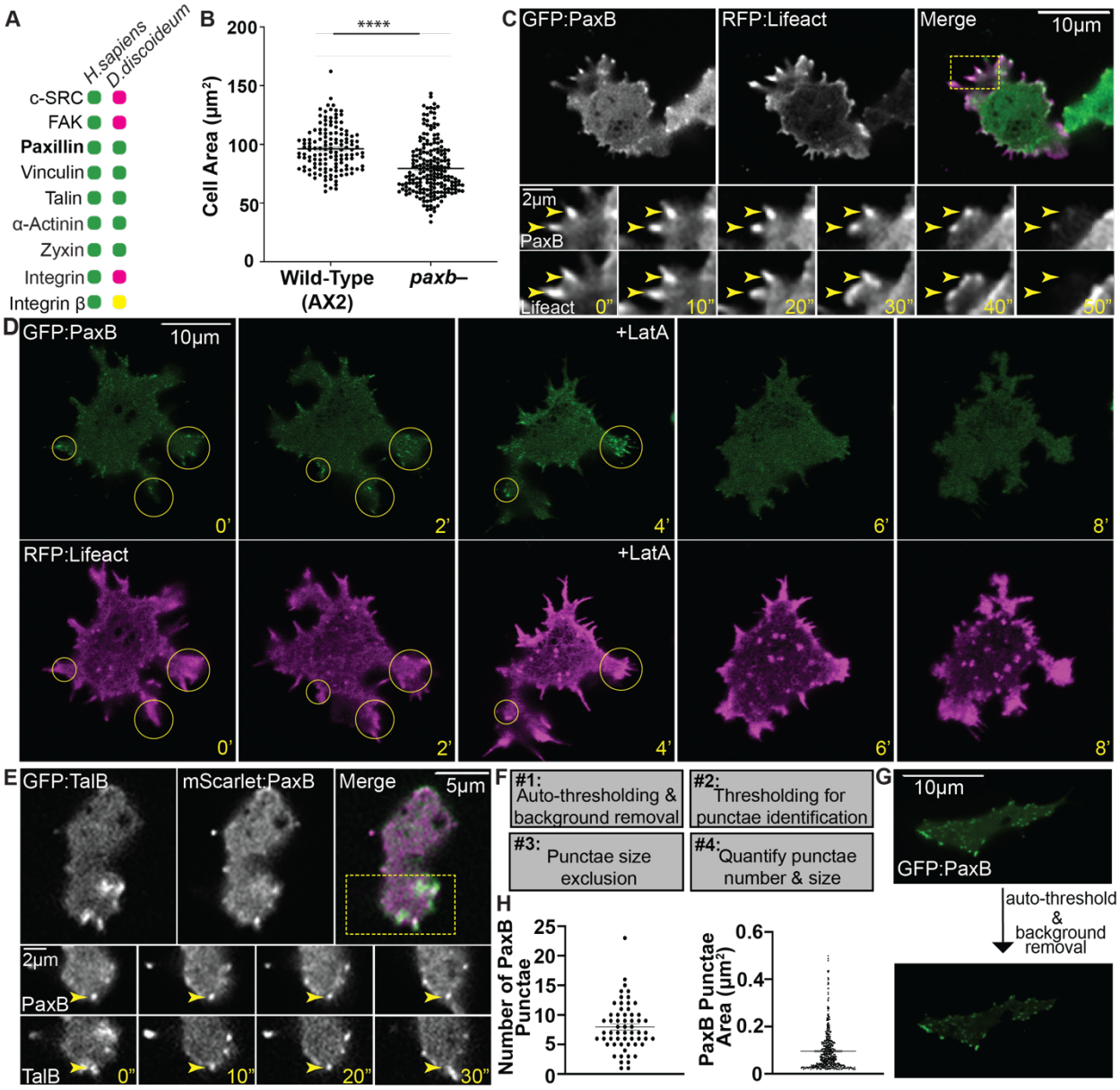

Figure 1: PaxillinB, the putative *Dictyostelium discoideum* homologue of the core adhesion scaffold Paxillin, forms small, short-lasting adhesion structures at the cell ventral surface. **A)** Comparison of the presence and absence of core focal adhesion components between humans and the model Amoebozoa, *Dictyostelium discoideum*. Green indicates presence of putative homologue, yellow indicates potential putative homologue, and pink indicates no putative homologue. Note that while *Dictyostelium* lacks putative orthologues of some components such as c-SRC and FAK, it possesses homologues of various core scaffolding components including Paxillin. **B)** Average whole cell area of wildtype and *paxb– Dictyostelium* cells as a proxy for adhesive capability. Student t-test, **** $p<0.0001$. n= 136 (AX2) and 202 (*paxb*-) cells across n=2 biological replicates. **C)** Representative timelapse fluorescent confocal microscopy images of *paxb*-/act15/GFP:PaxB;RFP:Lifeact *Dictyostelium* cells. Yellow arrowheads shown on inset images show presence and disassembly of co-localizing PaxillinB and actin punctae over time. Time indicated in seconds. **D)** Representative timelapse fluorescent confocal microscopy images

of act15/GFP:TalB;mScarlet:PaxB. Inset images demonstrate co-localization of PaxillinB and TalinB punctae, as indicated by yellow arrowhead. **E)** Schematic showing workflow of image processing pipeline for PaxillinB punctae identification and quantification. See Methods for details. **F)** Representative images prior to (top) and after (below) application of whole cell autothresholding and background removal to increase signal to noise ratio for PaxillinB punctae quantification. **G)** Quantification of PaxillinB punctae number per cell (left) and average area of individual PaxillinB punctae (right) using pipeline described in **E;** n=59 cells for left graph and n=505 punctae for right graph. Mean +/- SEM. **H)** Representative timelapse fluorescent confocal microscopy images of PaxillinB (top row) and actin (bottom row) in act15/GFP:PaxB;RFP:Lifeact *Dictyostelium* cells before and after spike-in of 1 uM LatrunculinA (LatA) during imaging. Time indicated in minutes. Spike-in of LatA indicated in image taken at 4-minute mark. Yellow circles in first three frames indicate sites of PaxB-positive punctae.

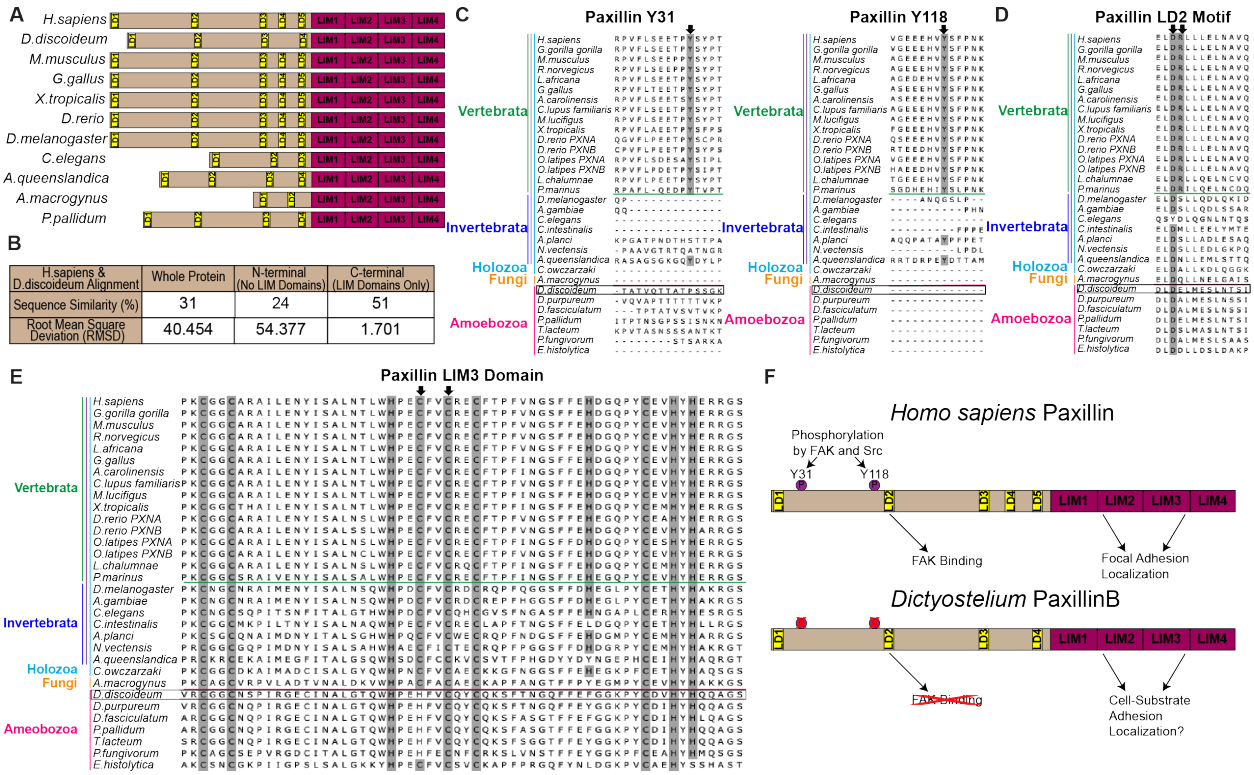

H.sapiens & D.discoideum Alignment	Whole Protein	N-terminal (No LIM Domains)	C-terminal (LIM Domains Only)
Sequence Similarity (%)	31	24	51
Root Mean Square Deviation (RMSD)	40.454	54.377	1.701

Figure 2: PaxillinB has conserved C-terminal LIM domains, but does not exhibit conservation of key N-terminal residues.

A) Schematic of Paxillin protein structure/domains across representative organisms. Note that all putative Paxillin molecules possess four C-terminal LIM domains but vary in N-terminal sequence length and LD motif number. **B)** Quantification of sequence (percent similarity) and structural (using root mean square deviation (RMSD) of Alphafold predicted structures) conservation between aligned human and *Dictyostelium* Paxillin molecules. Note substantial increased conservation of the C-terminal LIM domains as given by a higher percent sequence similarity and decreased RMSD value. **C)** Multiple Sequence Alignments (MSAs) of Paxillin Tyrosine 31 and 118, phosphorylation sites associated with focal adhesion turnover in Metazoans. Black arrowheads point to the tyrosine residues of interest. **D)** MSAs of Paxillin LD2 motifs, a known binding site for FAK in Metazoan adhesions. Black arrowheads indicate aspartic acid and arginine residues shown to be pivotal for FAK binding in Metazoan literature. **E)** MSAs of Paxillin LIM3 domains, which has been shown to be necessary for Paxillin localization to Metazoan focal adhesions. Cysteine and histidine residues are highlighted in gray, respectively. Black arrowheads indicate conservation of either a cysteine or histidine at key sites corresponding to zinc-coordinating residues pivotal for proper Paxillin localization. **F)** Schematic showing comparison of presence and absence of conserved adhesion-specific Paxillin domains between mammalian and *Dictyostelium* Paxillin molecules.

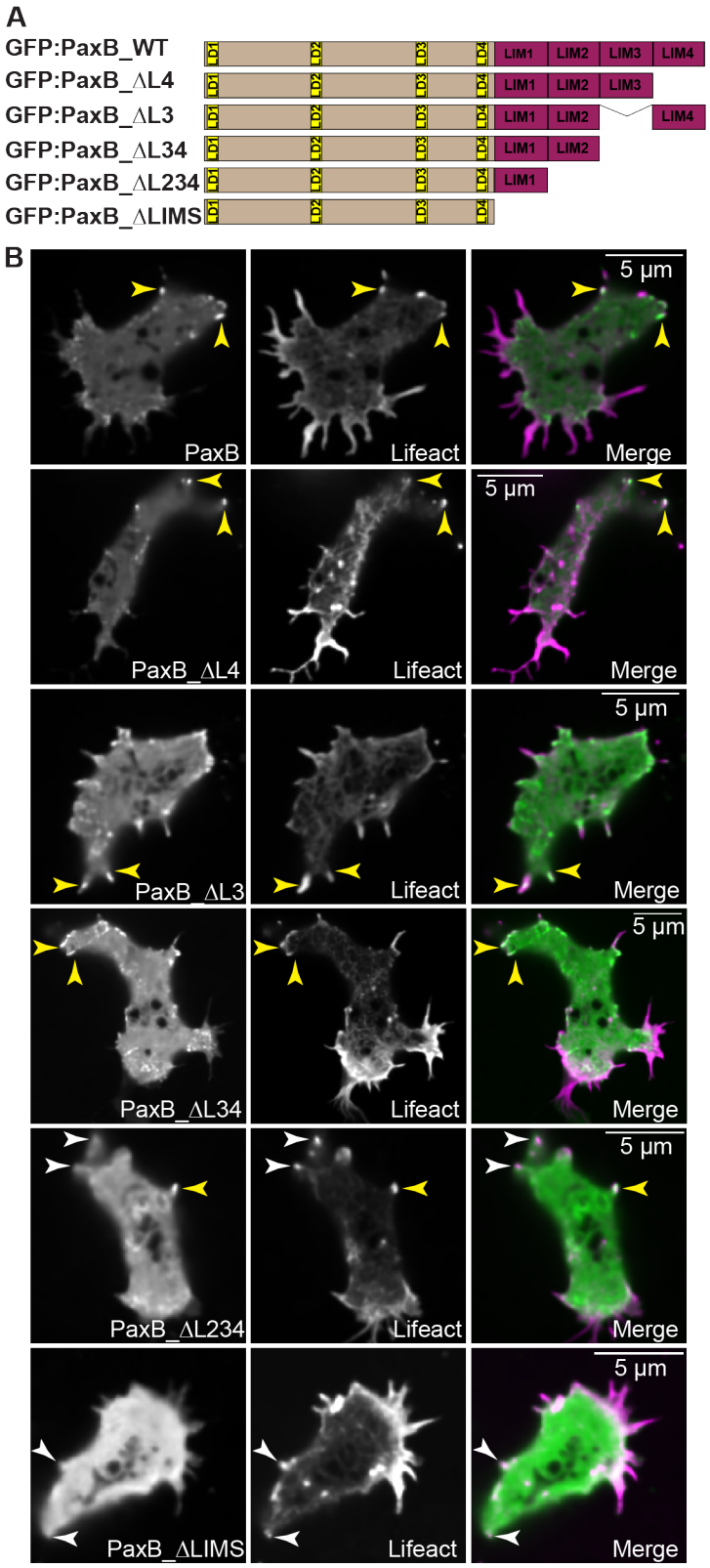

Figure 3: Perturbation of PaxillinB LIM3 domain alone is not sufficient to disrupt PaxillinB localization to cell-substrate adhesions

A) Schematic demonstrating wild-type and LIM domain-truncated PaxillinB molecules that were overexpressed in *paxb- Dictyostelium* cells. **B)** Representative images of timelapse fluorescent confocal microscopy of *paxb- Dictyostelium* cells overexpressing the PaxillinB molecules shown in **A.** Yellow arrowheads point to actin punctae that colocalizes with PaxillinB punctae. White arrowheads point to sites of actin punctae without co-localizing PaxillinB, suggesting perturbation of localization of PaxillinB to sites of cell-substrate adhesions.

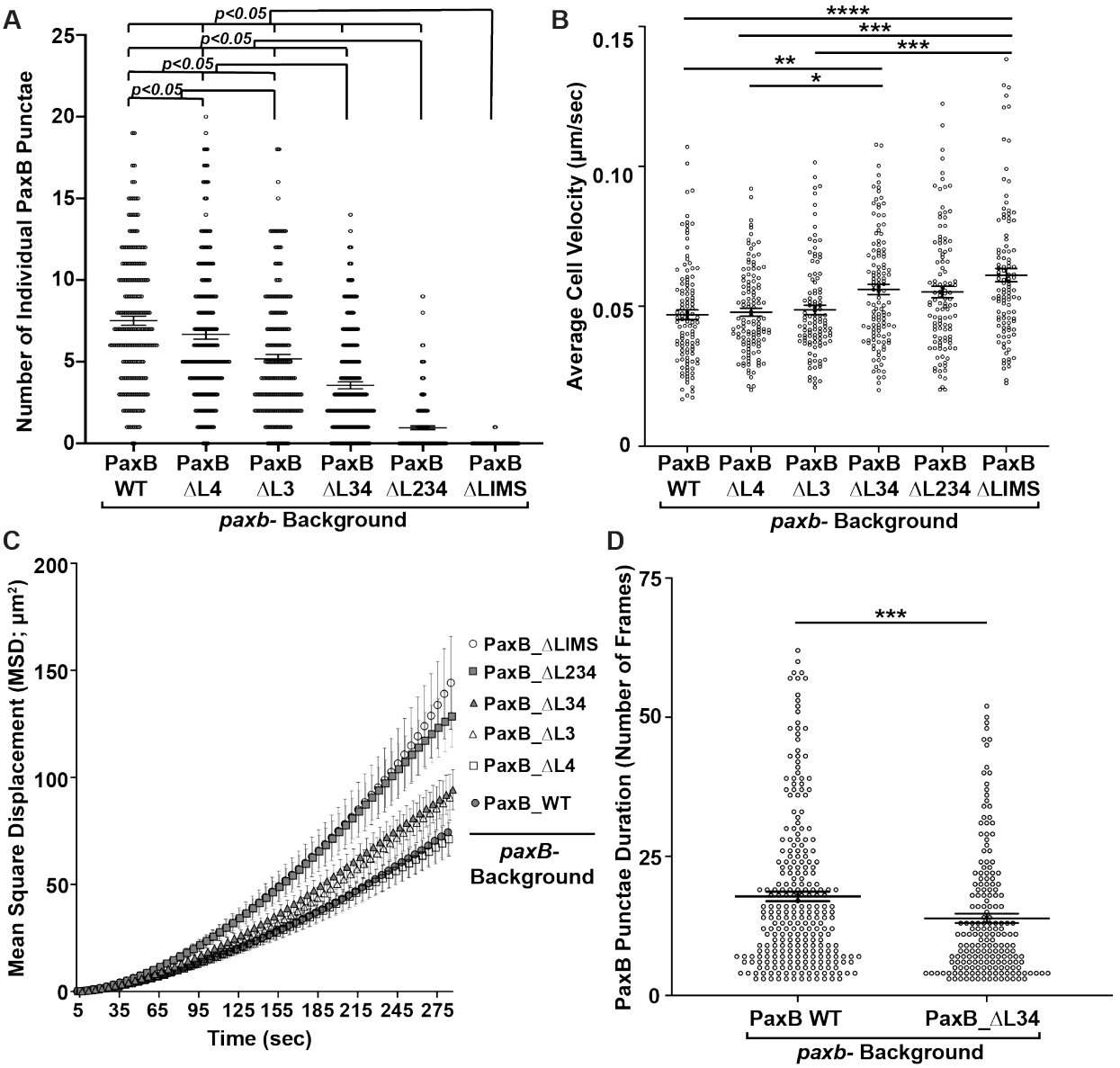

Figure 4: Perturbation of PaxillinB LIM domains decreases PaxillinB localization and stability at cell-substrate adhesions but increases cell migration velocity and persistence.
A) Quantification of number of PaxillinB punctae per cell in *Dictyostelium* cells overexpressing PaxillinB molecules shown in **Figure 3A.** n = 211 (PaxB-WT), 209 (PaxB-ΔL4), 203 (PaxB-ΔL3), 211 (PaxB-ΔL34), 210 (PaxB-ΔL234), and 213 (PaxB-ΔLIMS) cells across n=3 biological replicates per cell line. **B, C)** Quantification of average cell velocity **(B)** and mean square displacement **(C)** of randomly migrating *Dictyostelium* cells overexpressing PaxillinB molecules shown in **Figure 3A.** * p<0.05; *** p<0.001; **** p<0.0001. Mean +/- SEM. For both **B)** and **C),** n = 113 (PaxB-WT), 119 (PaxB-ΔL4), 108 (PaxB-ΔL3), 119 (PaxB-ΔL34), 111 (PaxB-ΔL234), and 108 (PaxB-ΔLIMS) cells across n=6 biological replicates per cell line. For **A-C)** graphs: Mean +/- SEM; For **A and B)** Kruskal-Wallis Test was used to determine statistical significance; Only statistically significant differences between cell lines are shown on graph; all other differences between cell lines are non-significant. **D)** Quantification of PaxillinB punctae duration during timelapse imaging of *Dictyostelium* cells overexpressing wildtype PaxillinB (PaxB-WT) or

truncated PaxillinB missing the LIM3 and LIM4 domain (PaxB-ΔL34). n = 264 (PaxB-WT) and 195 (PaxB-ΔL34) punctae across n=3 biological replicates per cell line. Student t-test, ** $p<0.01$ Mean +/- SEM.

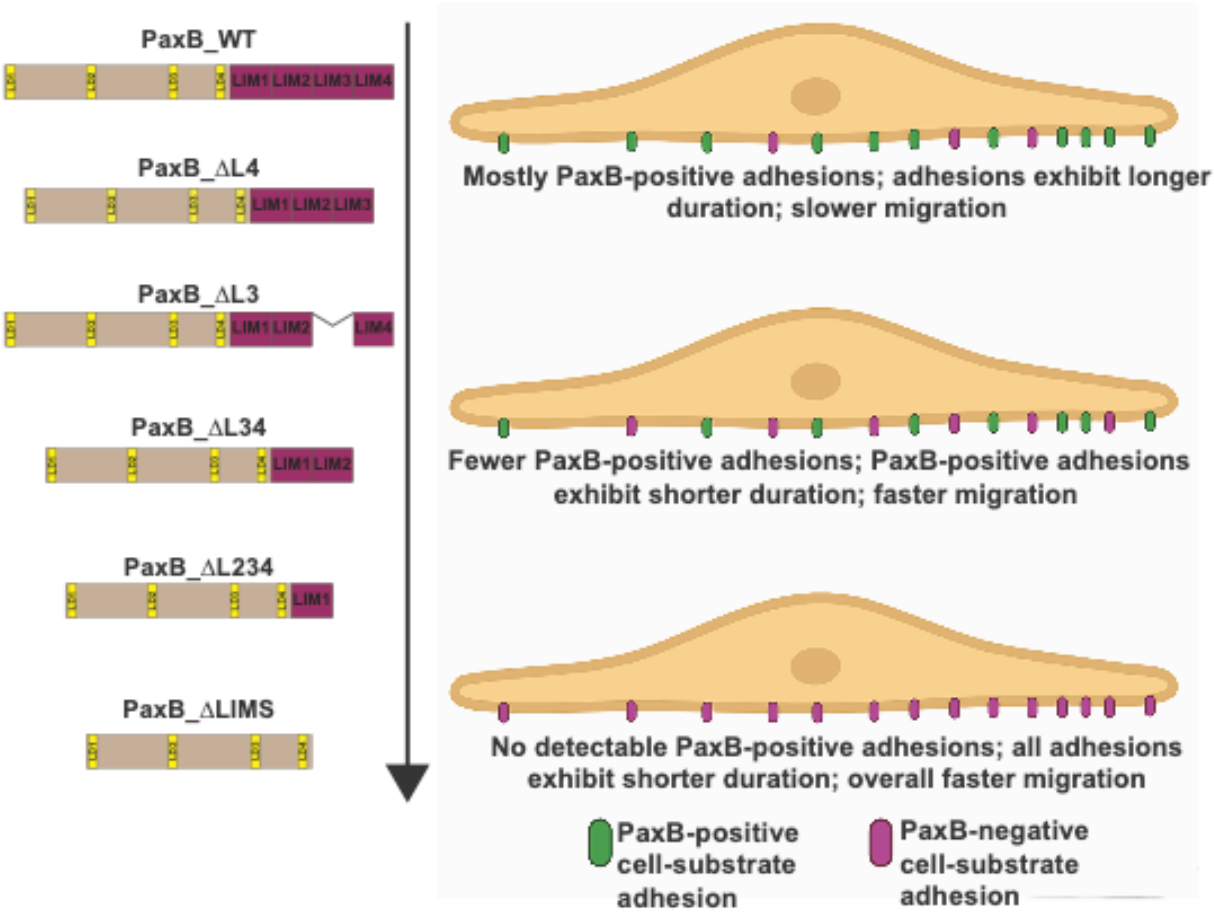

Figure 5: Proposed model: PaxillinB regulates *Dicytostelium* cell migration speed by stabilizing cell-substrate adhesion structures.
Increased truncations of the PaxillinB LIM domains leads to decreased localization of PaxillinB to *Dictyostelium* cell-substrate adhesions. As PaxillinB localization to cell-substrate adhesions decreases, the duration of cell-substrate adhesions decreases, leading to increased cell migration velocities and persistence.

724 **METHODS**
725
726 ***Dictyostelium* cell culturing**
727 Wild-type AX2 and *paxB- Dictyostelium* cells were obtained from the Dictyostelium Stock Center
728 (DSC) and cultured axenically at 21°C in HL5 media (Froquet et al., 2009) supplemented with
729 300 µg/mL Streptomycin Sulfate (Gold Biotechnology) on 10 cm plates. Null cells were selected
730 for with supplementation of 10 µg/mL Blasticidin S (Thermofisher). Transformed cells (see
731 Generation of Transgenic Lines), were selected for with additional supplementation of 20 µg/mL
732 G418 Sulfate (Thermofisher) and/or 50 µg/mL Hygromycin B (Thermofisher).
733
734 **Generation of expression plasmids**
735 The wild-type GFP:PaxillinB, RFP:Lifeact, and GFP:TalinB plasmids were gifts from Dr.
736 Margaret A. Titus (University of Minnesota).
737
738 **Cloning of mScarlet:PaxillinB construct**
739 To generate the mScarlet:PaxillinB plasmid expressed in **Figure 1D**, we amplified PaxillinB from
740 the GFP:PaxillinB plasmid for insertion into an mScarlet backbone vector, courtesy of Dr.
741 Margaret A. Titus, using Gibson assembly. To amplify GFP:PaxillinB (referred to as fragment A1
742 for Gibson assembly), we used primers A1-PaxillinB-F and A1-PaxillinB-R (Tm = 68°C). To
743 generate mScarlet backbone fragments (referred to as fragments A2 and A3) for Gibson assembly,
744 we used primers A2-mScarlet-Backbone-F and A2-mScarlet-Backbone-R (Tm = 61°C) for
745 fragment A2 and primers A3-mScarlet-Backbone-F and A3-mScarlet-Backbone-R (Tm = 69°C)
746 for fragment A3. PCR fragments were amplified in triplicate using NEB High Fidelity PCR Master
747 Mix with HF Buffer (M0531S), pooled and gel purified using Zymo Gel DNA Recovery Kits
748 (D4002) followed by ethanol precipitation to increase DNA fragment purity. Fragments were
749 Gibson assembled using NEBuilder HiFi DNA Assembly Master Mix (NEB E2621S). Whole
750 plasmid sequencing was performed by Plasmidsaurus using Oxford Nanopore Technology with
751 custom analysis and annotation.
752
753 Primer A1-PaxillinB-F: 5'-
754 GGTCCAGGTAAGGATCCAATGGCAACAAAAGGATTAAATATG-3'. Primer A1-
755 PaxillinB-R: 5'-
756 TTTAACTAGCTTAAGCAAATAATTTATTATGACAACCTTTACAATATG-3'. Primer A2-
757 mScarlet-Backbone-F: 5'-
758 TTGCTTAAGCTAGTTAAATAAATAAATTATTTAATAAATAAT-3'. Primer A2-mScarlet-
759 Backbone-R: 5'-AATGATGAGCACTTTTAAAGTTCTGCTATG-3'. Primer A3-mScarlet-
760 Backbone-F: 5'-AAAGTGCTCATCATTGGAAAACGTTCTTCG-3'. Primer A3-mScarlet-
761 Backbone-R: 5'-TGGATCCTTACCTGGACCTTTGTATAATTCATCCATACCACC-3'.
762
763 **Cloning of truncated PaxillinB constructs**
764 To generate plasmids possessing the truncated PaxillinB molecules outlined in **Figure 3A,** we used
765 the wild-type GFP:PaxillinB as a template to generate backbone and truncated PaxillinB insert
766 fragments for Gibson assembly. For all plasmids, four fragments were amplified for Gibson
767 assembly. For all truncated PaxillinB plasmids, the B3-GFP:PaxB-ALL and B4-GFP:PaxB-ALL
768 backbone fragments were amplified using the B3-GFP-PaxillinB-ALL-F and B3-GFP-PaxillinB-
769 ALL-R primers (Tm = 72°C) for the B3-GFP:PaxB-ALL backbone fragment and the B4-GFP-

PaxillinB-ALL-F and 43-GFP-PaxillinB-ALL-R (Tm = 72ºC) for the B4-GFP:PaxB-ALL backbone fragment.

For the GFP:PaxB-ΔL4 plasmid, fragments B1-GFP:PaxB-ΔL4 and B2-GFP:PaxB-ΔL4 were amplified using the B1-GFP-PaxillinB-ALL-F and B1-GFP-PaxillinB-ΔL4-R primers (Tm = 72ºC) for the B1-GFP:PaxB-ΔL4 fragment and the B2-GFP-PaxillinB-ΔL4-F and B2-GFP-PaxillinB-ALL-R primers (Tm = 72ºC) for the B2-GFP:PaxB-ΔL4 fragment.

For the GFP:PaxB-ΔL3 plasmid, fragments B1-GFP:PaxB-ΔL3 and B2-GFP:PaxB-ΔL3 were amplified using the B1-GFP-PaxillinB-ALL-F and B1-GFP-PaxillinB-ΔL3-R primers (Tm = 72ºC) for the B1-GFP:PaxB-ΔL3 fragment and the B2-GFP-PaxillinB-ΔL3-F and B2-GFP-PaxillinB-ALL-R primers (Tm = 72ºC) for the B2-GFP:PaxB-ΔL3 fragment.

For the GFP:PaxB-ΔL34 plasmid, fragments B1-GFP:PaxB-ΔL34 and B2-GFP:PaxB-ΔL34 were amplified using the B1-GFP-PaxillinB-ALL-F and B1-GFP-PaxillinB-ΔL34-R primers (Tm = 72ºC) for the B1-GFP:PaxB-ΔL34 fragment and the B2-GFP-PaxillinB-ΔL34-F and B2-GFP-PaxillinB-ALL-R primers (Tm = 72ºC) for the B2-GFP:PaxB-ΔL34 fragment.

For the GFP:PaxB-ΔL234 plasmid, fragments B1-GFP:PaxB-ΔL234 and B2-GFP:PaxB-ΔL234 were amplified using the B1-GFP-PaxillinB-ALL-F and B1-GFP-PaxillinB-ΔL234-R primers (Tm = 72ºC) for the B1-GFP:PaxB-ΔL234 fragment and the B2-GFP-PaxillinB-ΔL234-F and B2-GFP-PaxillinB-ALL-R primers (Tm = 72ºC) for the B2-GFP:PaxB-ΔL234 fragment.

For the GFP:PaxB-ΔLIMS plasmid, fragments B1-GFP:PaxB-ΔLIMS and B2-GFP:PaxB-ΔLIMS were amplified using the B1-GFP-PaxillinB-ALL-F and B1-GFP-PaxillinB-ΔLIMS-R primers (Tm = 72ºC) for the B1-GFP:PaxB-ΔLIMS fragment and the B2-GFP-PaxillinB-ΔLIMS-F and B2-GFP-PaxillinB-ALL-R primers (Tm = 72ºC) for the B2-GFP:PaxB-ΔLIMS fragment.

PCR fragments were amplified in triplicate using NEB High Fidelity PCR Master Mix with HF Buffer (M0531S), pooled and gel purified using Zymo Gel DNA Recovery Kits (D4002) followed by ethanol precipitation to increase DNA fragment purity. Fragments were Gibson assembled using NEBuilder HiFi DNA Assembly Master Mix (NEB E2621S). Whole plasmid sequencing was performed by Plasmidsaurus using Oxford Nanopore Technology with custom analysis and annotation.

Primer B1-GFP-Paxillin-ALL-F: 5'-AATCATGCGAAACGATCCAGCTTGAACATCTTCACCATCC-3'. Primer B1-GFP-PaxillinB-ΔL4-R: 5'-CTCTAGCGAGCTCTTAGCCAGCTTGTTGATGATAATGGACATCACAATAT-3'. Primer B1-GFP-PaxillinB-ΔL3-R: 5'-CAAACTGAAACGGCAAATGTTGAATAGAAATCGGCCTCAC-3'. Primer B1-GFP-PaxillinB-ΔL34-R: 5'-TCTAGCGAGCTCTTAAACGGCAAATGTTGAATAGAAATCGG-3'. Primer B1-GFP-PaxillinB-ΔL234-R: 5'-TCTAGCGAGCTCTTAAAACAATTCTTGATAACATTTTTCAC-3'. Primer B1-GFP-PaxillinB-ΔLIMS-R: 5'-

TAGCGAGCTCTTAACGTGATGTTGGTCCTGTTGAATCAATATCT-3'. Primer B2-GFP-PaxillinB-ΔL4-F: 5'-CAAGCTGGCTAAGAGCTCGCTAGAGTCGTCCATCAAT-3'. Primer B2-GFP-PaxillinB-ΔL3-F: 5'-ACATTTGCCGTTTCAGTTTGTTCTGGCTGTGGAAAAG-3'. Primer B2-GFP-PaxillinB-ΔL34-F: 5'-CCGTTTAAGAGCTCGCTAGAGTCGTCCATCAATTG-3'. Primer B2-GFP-PaxillinB-ΔL234-F: 5'-GTTTTAAGAGCTCGCTAGAGTCGTCCATCAATTGTTC-3'. Primer B2-GFP-PaxillinB-ΔLIMS-F: 5'-CATCACGTTAAGAGCTCGCTAGAGTCGTCCATCAATTG-3'. Primer B2-GFP-PaxillinB-ALL-R: 5'-ATAGTTGCCTGACTCCCCGTCGTGTAGATAACTACGATAC-3'. Primer B3-GFP-PaxillinB-ALL-F: 5'-AGTCAGGCAACTATGGATGAACGAAATAGACAGATCGCTG-3'. Primer B3-GFP-PaxillinB-ALL-R: 5'-CCGAATCATTGAAACATGGAGGGCAAAGTTTAGAATTAATAACAAC-3'. Primer B4-GFP-PaxillinB-ALL-F: 5'-GCCCTCCATGTTTCAATGATTCGGTAATCAACAAGAAGTGTG-3'. Primer B4-GFP-PaxillinB-ALL-R: 5'-TCAAGCTGGATCGTTTCGCATGATTGAACAAGATGGATTG-3'.

Generation of transgenic lines

Dictyostelium cells were transformed via electroporation as previously described (Gaudet et al., 2007). Briefly, axenic cells were cultured in HL5, harvested, pelleted and washed twice with ice-cold H-50 buffer (20 mM HEPES, 50 mM KCl, 1 mM $MgSO_4$, 10 mM NaCl, 5 mM $NaHCO_3$ and 1 mM $NaH_2PO_4 \cdot 2H_2O$). Cells were resuspended in H-50 at 1e8 cells/mL and 100 µl of cells were added to a 0.1 cm gap size cuvette with 15 µg of plasmid DNA for single construct transformations or 10 µg of plasmid DNA per construct for double construct transformation. Cells were electroporated via pulsing at 0.85 kV, 25 µF and 0.6 ms τ twice, with a 5 second pause in between pulses. Cells were rested on ice for 5 minutes post-electroporation before being added to 10 cm plates with fresh HL5 media supplemented with 300 µg/mL Streptomycin Sulfate for 24 hours for recovery. After 24 hours, cells were moved to selection media with 20 µg/mL G418 Sulfate and/or 50 µg/mL Hygromycin B. If null cells were used as a background, 10 µg/mL Blasticidin S was also added to the selection media.

Preparation of *Dictyostelium* cells for imaging

Dictyostelium cells were cultured in HL5 media on 10 cm plates to a confluency of 1-2e6 cells/mL, as measured via Countess II FL (Thermofisher), and a minimum of 10 mLs were harvested. Cells were centrifuged at 600 rpm for 5 minutes at 4°C and resuspended in Development Buffer (DB; 5 mM Na_2HPO_4, 5 mM KH_2PO_4, 1 mM $CaCl_2$, 2 mM $MgCl_2$, pH=6.5) at a concentration of $2.5e^6$ cells/mL. $1e^7$ total cells were plated in a 6 cm plate and allowed to adhere for 30 minutes before being rinsed twice with 2 mL DB and allowed to develop for 3.5 hours. After 3.5 hours, cells were resuspended and 45 µL of cells were added to 955 µL of DB and placed in a 35 mm glass bottom dish (FD35-100, World Precision Instruments) for imaging.

***Dictyostelium* imaging**

Spinning disc confocal fluorescence microscopy was done using either a Leica HC PL APO 63×/1.40 oil immersion objective with 2× zoom on a Leica Yokogawa CSU-W1 spinning disc confocal scanner unit with iXon Life 888 EMCCD camera and VisiView software for spinning disc confocal microscopy **(for images and data generated for Figures 1B, 1D, 4B and 4C)** or a Nikon PLAN APO λD 60X/1.42 oil immersion objective with 1X zoom on a Nikon Ti2

microscope with a Yokogawa CSU-W1 spinning disc confocal scanner unit, Gataca Systems Live-SR super resolution module and Kinetix 22 Scientific CMOS (sCMOS) camera for super resolution spinning disc confocal microscopy with NIS AR software **(for images and data generated for Figures 1G, 1H, 3B, 4A, 4D, and S4A-D)**. Laser scanning confocal microscopy was done using Leica HC PL APO CS2 63×/1.40 oil immersion objective with 2X zoom on a Leica TCS SP8 laser confocal microscope with photomultiplier tubes (PMT) detectors and Leica Application Suite X software **(for images generated for Figure 1I).** TIRF microscopy was done using a Nikon 60X Apochromat TIRF oil objective with 1X zoom on a Nikon Ti2 microscope with Gataca Systems Ilas2 TIRF platform and iXon Ultra 897 EMCCD camera and NIS AR software **(for images generated for Figure S2)**. For all microscopy, *Dictyostelium* cells were in development buffer (DB).

LatrunculinA spike-in

Dictyostelium cells undergoing random cell migration were imaged in a single plane every 5 sec for 10 min. 1 ml of 2 μM LatrunculinA (Sigma Aldrich) was spiked-in to the imaging dish at the 4 min mark to bring the final concentration of LatrunculinA to 1 μM. Imaging was continued for the remaining 6 min to observe effect of spike-in.

***Dictyostelium* cell spreading**

Wild-type and *paxB- Dictyostelium* cells were captured using Differential Interference Contrast (DIC) microscopy. Image files were blinded using ImageJ's (Schindelin et al., 2012) Blind Analysis Tools and processed using the Trainable Weka Segmentation plug-in (Arganda-Carreras et al., 2017) on ImageJ to classify cells and create whole cell binary map. Cell area was subsequently measured using the Measurement tool on ImageJ.

Identification and quantification of PaxillinB punctae number and size

PaxillinB punctae were identified and quantified using a custom-made ImageJ processing pipeline. Briefly, fluorescent images of *Dictyostelium* cells expressing wild-type or truncated GFP-tagged PaxillinB were auto-thresholded and background noise was removed through ImageJ's NaN Background tool. After background removal, auto-threshold was performed again and the mean fluorescence intensity (MFI) and standard deviation (SD) was then measured for each cell. To identify and quantify punctae, thresholding was used with a value of MFI + 3 SD used as the lower limit and 65535 used as the upper limit. Punctae that identified via thresholding were then analyzed using the Analyze Particles command, filtering to keep punctae between 0.02 μm^2 and 0.5 μm^2. Total number of punctae per cell was displayed in the Summary table while individual punctae were displayed in the Results table after the pipeline was executed. The full macro for punctae identification and quantification is available on GitHub (https://github.com/rohjohnson-lab).

***Dictyostelium* cell migration analysis**

Dictyostelium cells undergoing random cell migration were imaged in a single plane every 5 sec for 5 min in the GFP channel. Migration was tracked using auto thresholding and binary tracking of whole cells in NIS-Elements AR Advanced 2D Tracking software. Final velocities were calculated by averaging the velocities between each time point of the time-lapse video. Mean square displacement was calculated using the DiPer computer program (Gorelik and Gautreau, 2014).

907 **PaxillinB punctae duration analysis**
908 On NIS-Elements AR, a "Regional Maxima" 3 x 3 kernel operation (Sysko and Davis, 2010) was
909 applied to timelapse videos of individual *Dictyostelium* cells undergoing random cell migration to
910 remove background noise and mitigate thresholding issues due to uneven illumination. Auto-
911 thresholding was applied to the whole video, as well as edge smoothing and clean-up to remove
912 single pixels, to define PaxillinB punctae as distinct binary objects. NIS-Elements AR Advanced
913 2D Tracking was then used to track binary duration – defined as the number of frames from a
914 punctae first forms and is identified to the last frame it is present and identified – as a proxy for
915 PaxillinB punctae duration. For Advanced 2D Tracking, punctae present in the first or last frame
916 of the video were removed and a minimum duration of three frames was required. Lastly, manual
917 curation of identified punctae was performed to remove any punctae binaries that merged or
918 skipped frames.
919
920 **Bidirectional homology queries**
921 For all bidirectional homology queries, we used the *Homo sapiens* α-Integrin, β-Integrin, Vinculin,
922 Talin, Zyxin, Paxillin, α-Actinin, c-SRC, and FAK protein sequences as initial queries. First,
923 sequence homology was done using the Protein basic local alignment search tool (BLASTp) to
924 blast the *H.sapiens* protein sequences against genomes of candidate organisms in the National
925 Center for Biotechnology Information (NCBI), Joint Genome Institute (JGI) and Ensembl genome
926 databases (Altschul et al., 1990; Martin et al., 2023; Nordberg et al., 2014), using an e-value
927 threshold of 10^{-10}. Reciprocal searches were performed using identified putative orthologue
928 sequences from candidate organisms against the *H.sapiens* genome. For structural homology,
929 predicted Alphafold structures (Jumper et al., 2021; Varadi et al., 2022) of the *H.sapiens* adhesion
930 molecules were used and structural homologs were searched for in candidate organisms using the
931 Foldseek (van Kempen et al., 2023) webserver with the AlphafoldDB/UniProt50 v4,
932 AlphafoldDB/Swiss-Prot v4, AlphafoldDB/Proteome v4, CATH50 4.3.0, Protein Data Bank
933 (PDB) 100 20231120, MGnify-ESM30 v1, and GMGCL 2204 databases (Berman et al., 2000;
934 Coelho et al., 2022; Knudsen and Wiuf, 2010; Richardson et al., 2023; Varadi et al., 2022) and
935 3Di/AA structural alignment methods. Reciprocal searches were performed using identified
936 putative orthologue structures from candidate organisms as the input query against *H.sapiens*
937 proteosome. For domain family-based analyses, we input the *H.sapiens* protein sequences into the
938 HMMER webserver (Potter et al., 2018) using the built-in pHMMER and HMMSCAN tools to
939 identify putative orthologues in candidate organisms and confirm domain architecture of input
940 queries, respectively. This process was repeated using identified putative orthologues from
941 candidate species to test for reciprocity to the *H.sapiens* genome and confirm predicted domain
942 architecture of candidate orthologue queries. If no homologs were detected using the *H.sapiens*
943 sequences or structures for a candidate organisms, queries were repeated using previously
944 identified putative orthologues from other organisms more closely related to the candidate
945 organisms in order to account for distant homology.
946
947 **Homology searches for LIM domain possessing proteins**
948 Methods described in the "Bidirectional homology queries" section were repeated, this time using
949 the *Homo sapiens* sequences and structures for Paxillin, Leupaxin, LIMS1, LIMS2, PDLIM7,
950 Testin and Zyxin as initial queries.
951
952

Multiple sequence alignments and phylogenetic analysis

Protein sequence were aligned using the MAFFT (Katoh and Standley, 2013) plug-in on Geneious Prime software (Dotmatics). A maximum likelihood (ML) phylogenetic tree was then inferred from the resulting multiple sequence alignment using PHYML (Guindon et al., 2010) plug-in with an LG substitution model and 100 bootstraps replicates. Trees were visualized using FigTree v1.4.4 software (http://tree.bio.ed.ac.uk/software/figtree/).

Paxillin structural analysis

PDB files for the predicted Alphafold structures of *H.sapiens* Paxillin and *D.discoideum* PaxillinB molecules were obtained from the Alphafold Protein Structure Database (Varadi et al., 2022). The PDB files were visualized in USCF ChimeraX software developed by the Resource for Biocomputing, Visualization, and Informatics at the University of California, San Francisco, with support from National Institutes of Health R01-GM129325 and the Office of Cyber Infrastructure and Computational Biology, National Institute of Allergy and Infectious Diseases (Meng et al., 2023). Structures were aligned using the Matchmaker feature and a Smith-Waterman alignment algorithm.

Graphical representation and statistical analysis

All graphs were generated from Prism (v8, GraphPad) and Excel (v16.43, Microsoft). Statistical and normality analyses were performed using Prism (v8, GraphPad). D'Agostino-Pearson, Shapiro-Wilk, Anderson-Darling and Kolmogorov-Smirnov normality tests were run prior to statistical analyses to test for normality of datasets. Outliers were identified by using mean +/- three standard deviations and removed for **Figures 1B, 1H (punctae number), 4A (except for columns GFP:PaxB-ΔL234 and GFP:PaxB-ΔLIMS) 4B, 4C and S4B.** For other graphs, outliers were not calculated because we had already defined criteria during pipeline analysis **(Figures 1H area, S4A)** or there was a large number of zero values **(>50%; Figure 4A columns GFP:PaxB-ΔL234 and GFP:PaxB-ΔLIMS).** N-values of biological replicates, the number of cells, and specific statistical tests used are found in the figure legends.

999 **REFERENCES**

1000

1001 Alexandrova, A.Y., A.S. Chikina, and T.M. Svitkina. 2020. Actin cytoskeleton in mesenchymal-to-
1002 amoeboid transition of cancer cells. *Int Rev Cell Mol Biol*. 356:197-256.
1003 Altschul, S.F., W. Gish, W. Miller, E.W. Myers, and D.J. Lipman. 1990. Basic local alignment
1004 search tool. *J Mol Biol*. 215:403-410.
1005 Arganda-Carreras, I., V. Kaynig, C. Rueden, K.W. Eliceiri, J. Schindelin, A. Cardona, and H.
1006 Sebastian Seung. 2017. Trainable Weka Segmentation: a machine learning tool for
1007 microscopy pixel classification. *Bioinformatics*. 33:2424-2426.
1008 Bellis, S.L., J.A. Perrotta, M.S. Curtis, and C.E. Turner. 1997. Adhesion of fibroblasts to
1009 fibronectin stimulates both serine and tyrosine phosphorylation of paxillin. *Biochem J*.
1010 325 (Pt 2):375-381.
1011 Beningo, K.A., M. Dembo, I. Kaverina, J.V. Small, and Y.L. Wang. 2001. Nascent focal adhesions
1012 are responsible for the generation of strong propulsive forces in migrating fibroblasts. *J*
1013 *Cell Biol*. 153:881-888.
1014 Berman, H.M., J. Westbrook, Z. Feng, G. Gilliland, T.N. Bhat, H. Weissig, I.N. Shindyalov, and P.E.
1015 Bourne. 2000. The Protein Data Bank. *Nucleic Acids Res*. 28:235-242.
1016 Brown, M.C., J.A. Perrotta, and C.E. Turner. 1996. Identification of LIM3 as the principal
1017 determinant of paxillin focal adhesion localization and characterization of a novel motif
1018 on paxillin directing vinculin and focal adhesion kinase binding. *J Cell Biol*. 135:1109-
1019 1123.
1020 Brunet, T., M. Albert, W. Roman, M.C. Coyle, D.C. Spitzer, and N. King. 2021. A flagellate-to-
1021 amoeboid switch in the closest living relatives of animals. *Elife*. 10.
1022 Bukharova, T., G. Weijer, L. Bosgraaf, D. Dormann, P.J. van Haastert, and C.J. Weijer. 2005.
1023 Paxillin is required for cell-substrate adhesion, cell sorting and slug migration during
1024 Dictyostelium development. *J Cell Sci*. 118:4295-4310.
1025 Burridge, K., C.E. Turner, and L.H. Romer. 1992. Tyrosine phosphorylation of paxillin and
1026 pp125FAK accompanies cell adhesion to extracellular matrix: a role in cytoskeletal
1027 assembly. *J Cell Biol*. 119:893-903.
1028 Cai, S., X. Liu, A. Glasser, T. Volberg, M. Filla, B. Geiger, J.R. Polansky, and P.L. Kaufman. 2000.
1029 Effect of latrunculin-A on morphology and actin-associated adhesions of cultured human
1030 trabecular meshwork cells. *Mol Vis*. 6:132-143.
1031 Caillier, A., D. Oleksyn, D.J. Fowell, J. Miller, and P.W. Oakes. 2023. T cells Use Focal Adhesions
1032 to Pull Themselves Through Confined Environments. *bioRxiv*.
1033 Callan-Jones, A.C., and R. Voituriez. 2016. Actin flows in cell migration: from locomotion and
1034 polarity to trajectories. *Curr Opin Cell Biol*. 38:12-17.
1035 Case, L.B., and C.M. Waterman. 2015. Integration of actin dynamics and cell adhesion by a
1036 three-dimensional, mechanosensitive molecular clutch. *Nat Cell Biol*. 17:955-963.
1037 Cassandri, M., A. Smirnov, F. Novelli, C. Pitolli, M. Agostini, M. Malewicz, G. Melino, and G.
1038 Raschella. 2017. Zinc-finger proteins in health and disease. *Cell Death Discov*. 3:17071.
1039 Choi, C.K., M. Vicente-Manzanares, J. Zareno, L.A. Whitmore, A. Mogilner, and A.R. Horwitz.
1040 2008. Actin and alpha-actinin orchestrate the assembly and maturation of nascent
1041 adhesions in a myosin II motor-independent manner. *Nat Cell Biol*. 10:1039-1050.

1042 Coelho, L.P., R. Alves, A.R. Del Rio, P.N. Myers, C.P. Cantalapiedra, J. Giner-Lamia, T.S. Schmidt,
1043 D.R. Mende, A. Orakov, I. Letunic, F. Hildebrand, T. Van Rossum, S.K. Forslund, S.
1044 Khedkar, O.M. Maistrenko, S. Pan, L. Jia, P. Ferretti, S. Sunagawa, X.M. Zhao, H.B.
1045 Nielsen, J. Huerta-Cepas, and P. Bork. 2022. Towards the biogeography of prokaryotic
1046 genes. *Nature*. 601:252-256.
1047 Copos, C.A., S. Walcott, J.C. Del Alamo, E. Bastounis, A. Mogilner, and R.D. Guy. 2017.
1048 Mechanosensitive Adhesion Explains Stepping Motility in Amoeboid Cells. *Biophys J*.
1049 112:2672-2682.
1050 Cornillon, S., R. Froquet, and P. Cosson. 2008. Involvement of Sib proteins in the regulation of
1051 cellular adhesion in Dictyostelium discoideum. *Eukaryot Cell*. 7:1600-1605.
1052 Cornillon, S., L. Gebbie, M. Benghezal, P. Nair, S. Keller, B. Wehrle-Haller, S.J. Charette, F.
1053 Bruckert, F. Letourneur, and P. Cosson. 2006. An adhesion molecule in free-living
1054 Dictyostelium amoebae with integrin beta features. *EMBO Rep*. 7:617-621.
1055 Cornillon, S., E. Pech, M. Benghezal, K. Ravanel, E. Gaynor, F. Letourneur, F. Bruckert, and P.
1056 Cosson. 2000. Phg1p is a nine-transmembrane protein superfamily member involved in
1057 dictyostelium adhesion and phagocytosis. *J Biol Chem*. 275:34287-34292.
1058 De Pascalis, C., and S. Etienne-Manneville. 2017. Single and collective cell migration: the
1059 mechanics of adhesions. *Mol Biol Cell*. 28:1833-1846.
1060 Devreotes, P.N., and S.H. Zigmond. 1988. Chemotaxis in eukaryotic cells: a focus on leukocytes
1061 and Dictyostelium. *Annu Rev Cell Biol*. 4:649-686.
1062 Du, F., A.V. Garg, K. Kosar, S. Majumder, D.G. Kugler, G.H. Mir, M. Maggio, M. Henkel, A. Lacy-
1063 Hulbert, and M.J. McGeachy. 2016. Inflammatory Th17 Cells Express Integrin
1064 alphavbeta3 for Pathogenic Function. *Cell Rep*. 16:1339-1351.
1065 Duran, M.B., A. Rahman, M. Colten, and D. Brazill. 2009. Dictyostelium discoideum paxillin
1066 regulates actin-based processes. *Protist*. 160:221-232.
1067 Fernandes, N.R.J., N.S. Reilly, D.C. Schrock, D.C. Hocking, P.W. Oakes, and D.J. Fowell. 2020.
1068 CD4(+) T Cell Interstitial Migration Controlled by Fibronectin in the Inflamed Skin. *Front*
1069 *Immunol*. 11:1501.
1070 Fey, P., S. Stephens, M.A. Titus, and R.L. Chisholm. 2002. SadA, a novel adhesion receptor in
1071 Dictyostelium. *J Cell Biol*. 159:1109-1119.
1072 Fierro Morales, J.C., Q. Xue, and M. Roh-Johnson. 2022. An evolutionary and physiological
1073 perspective on cell-substrate adhesion machinery for cell migration. *Front Cell Dev Biol*.
1074 10:943606.
1075 Friedl, P., S. Borgmann, and E.B. Brocker. 2001. Amoeboid leukocyte crawling through
1076 extracellular matrix: lessons from the Dictyostelium paradigm of cell movement. *J*
1077 *Leukoc Biol*. 70:491-509.
1078 Friedl, P., F. Entschladen, C. Conrad, B. Niggemann, and K.S. Zanker. 1998. CD4+ T lymphocytes
1079 migrating in three-dimensional collagen lattices lack focal adhesions and utilize beta1
1080 integrin-independent strategies for polarization, interaction with collagen fibers and
1081 locomotion. *Eur J Immunol*. 28:2331-2343.
1082 Friedl, P., and K. Wolf. 2010. Plasticity of cell migration: a multiscale tuning model. *J Cell Biol*.
1083 188:11-19.
1084 Fritz-Laylin, L.K., S.J. Lord, and R.D. Mullins. 2017. WASP and SCAR are evolutionarily conserved
1085 in actin-filled pseudopod-based motility. *J Cell Biol*. 216:1673-1688.

1086 Fritz-Laylin, L.K., and M.A. Titus. 2023. The evolution and diversity of actin-dependent cell
1087 migration. *Mol Biol Cell*. 34:pe6.
1088 Froquet, R., M. le Coadic, J. Perrin, N. Cherix, S. Cornillon, and P. Cosson. 2012. TM9/Phg1 and
1089 SadA proteins control surface expression and stability of SibA adhesion molecules in
1090 Dictyostelium. *Mol Biol Cell*. 23:679-686.
1091 Froquet, R., E. Lelong, A. Marchetti, and P. Cosson. 2009. Dictyostelium discoideum: a model
1092 host to measure bacterial virulence. *Nat Protoc*. 4:25-30.
1093 Fukui, Y., and S. Inoue. 1997. Amoeboid movement anchored by eupodia, new actin-rich
1094 knobby feet in Dictyostelium. *Cell Motil Cytoskeleton*. 36:339-354.
1095 Gardel, M.L., I.C. Schneider, Y. Aratyn-Schaus, and C.M. Waterman. 2010. Mechanical
1096 integration of actin and adhesion dynamics in cell migration. *Annu Rev Cell Dev Biol*.
1097 26:315-333.
1098 Gaudet, P., K.E. Pilcher, P. Fey, and R.L. Chisholm. 2007. Transformation of Dictyostelium
1099 discoideum with plasmid DNA. *Nat Protoc*. 2:1317-1324.
1100 Gaylo-Moynihan, A., H. Prizant, M. Popovic, N.R.J. Fernandes, C.S. Anderson, K.K. Chiou, H. Bell,
1101 D.C. Schrock, J. Schumacher, T. Capece, B.L. Walling, D.J. Topham, J. Miller, A.V. Smrcka,
1102 M. Kim, A. Hughson, and D.J. Fowell. 2019. Programming of Distinct Chemokine-
1103 Dependent and -Independent Search Strategies for Th1 and Th2 Cells Optimizes
1104 Function at Inflamed Sites. *Immunity*. 51:298-309 e296.
1105 Geiger, B., J.P. Spatz, and A.D. Bershadsky. 2009. Environmental sensing through focal
1106 adhesions. *Nat Rev Mol Cell Biol*. 10:21-33.
1107 Gorelik, R., and A. Gautreau. 2014. Quantitative and unbiased analysis of directional persistence
1108 in cell migration. *Nat Protoc*. 9:1931-1943.
1109 Guindon, S., J.F. Dufayard, V. Lefort, M. Anisimova, W. Hordijk, and O. Gascuel. 2010. New
1110 algorithms and methods to estimate maximum-likelihood phylogenies: assessing the
1111 performance of PhyML 3.0. *Syst Biol*. 59:307-321.
1112 Guler, B.E., J. Krzysko, and U. Wolfrum. 2021. Isolation and culturing of primary mouse
1113 astrocytes for the analysis of focal adhesion dynamics. *STAR Protoc*. 2:100954.
1114 Han, S.J., E.V. Azarova, A.J. Whitewood, A. Bachir, E. Guttierrez, A. Groisman, A.R. Horwitz, B.T.
1115 Goult, K.M. Dean, and G. Danuser. 2021. Pre-complexation of talin and vinculin without
1116 tension is required for efficient nascent adhesion maturation. *Elife*. 10.
1117 Han, S.J., Y. Oak, A. Groisman, and G. Danuser. 2015. Traction microscopy to identify force
1118 modulation in subresolution adhesions. *Nat Methods*. 12:653-656.
1119 Hibi, M., A. Nagasaki, M. Takahashi, A. Yamagishi, and T.Q. Uyeda. 2004. Dictyostelium
1120 discoideum talin A is crucial for myosin II-independent and adhesion-dependent
1121 cytokinesis. *J Muscle Res Cell Motil*. 25:127-140.
1122 Hu, Y.L., S. Lu, K.W. Szeto, J. Sun, Y. Wang, J.C. Lasheras, and S. Chien. 2014. FAK and paxillin
1123 dynamics at focal adhesions in the protrusions of migrating cells. *Sci Rep*. 4:6024.
1124 Hynes, R.O., and Q. Zhao. 2000. The evolution of cell adhesion. *J Cell Biol*. 150:F89-96.
1125 Illergard, K., D.H. Ardell, and A. Elofsson. 2009. Structure is three to ten times more conserved
1126 than sequence--a study of structural response in protein cores. *Proteins*. 77:499-508.
1127 Iwadate, Y., and S. Yumura. 2008a. Actin-based propulsive forces and myosin-II-based
1128 contractile forces in migrating Dictyostelium cells. *J Cell Sci*. 121:1314-1324.

1129 Iwadate, Y., and S. Yumura. 2008b. Molecular dynamics and forces of a motile cell
1130 simultaneously visualized by TIRF and force microscopies. *Biotechniques*. 44:739-750.
1131 Jahnel, S.M., M. Walzl, and U. Technau. 2014. Development and epithelial organisation of
1132 muscle cells in the sea anemone Nematostella vectensis. *Front Zool*. 11:44.
1133 Jamerson, M., B. da Rocha-Azevedo, G.A. Cabral, and F. Marciano-Cabral. 2012. Pathogenic
1134 Naegleria fowleri and non-pathogenic Naegleria lovaniensis exhibit differential adhesion
1135 to, and invasion of, extracellular matrix proteins. *Microbiology (Reading)*. 158:791-803.
1136 Jannat, R.A., G.P. Robbins, B.G. Ricart, M. Dembo, and D.A. Hammer. 2010. Neutrophil adhesion
1137 and chemotaxis depend on substrate mechanics. *J Phys Condens Matter*. 22:194117.
1138 Jumper, J., R. Evans, A. Pritzel, T. Green, M. Figurnov, O. Ronneberger, K. Tunyasuvunakool, R.
1139 Bates, A. Zidek, A. Potapenko, A. Bridgland, C. Meyer, S.A.A. Kohl, A.J. Ballard, A. Cowie,
1140 B. Romera-Paredes, S. Nikolov, R. Jain, J. Adler, T. Back, S. Petersen, D. Reiman, E.
1141 Clancy, M. Zielinski, M. Steinegger, M. Pacholska, T. Berghammer, S. Bodenstein, D.
1142 Silver, O. Vinyals, A.W. Senior, K. Kavukcuoglu, P. Kohli, and D. Hassabis. 2021. Highly
1143 accurate protein structure prediction with AlphaFold. *Nature*. 596:583-589.
1144 Kanchanawong, P., G. Shtengel, A.M. Pasapera, E.B. Ramko, M.W. Davidson, H.F. Hess, and C.M.
1145 Waterman. 2010. Nanoscale architecture of integrin-based cell adhesions. *Nature*.
1146 468:580-584.
1147 Katoh, K., and D.M. Standley. 2013. MAFFT multiple sequence alignment software version 7:
1148 improvements in performance and usability. *Mol Biol Evol*. 30:772-780.
1149 Kim, D.H., and D. Wirtz. 2013. Focal adhesion size uniquely predicts cell migration. *FASEB J*.
1150 27:1351-1361.
1151 Knudsen, M., and C. Wiuf. 2010. The CATH database. *Hum Genomics*. 4:207-212.
1152 Kunwar, P.S., D.E. Siekhaus, and R. Lehmann. 2006. In vivo migration: a germ cell perspective.
1153 *Annu Rev Cell Dev Biol*. 22:237-265.
1154 Lammermann, T., B.L. Bader, S.J. Monkley, T. Worbs, R. Wedlich-Soldner, K. Hirsch, M. Keller, R.
1155 Forster, D.R. Critchley, R. Fassler, and M. Sixt. 2008. Rapid leukocyte migration by
1156 integrin-independent flowing and squeezing. *Nature*. 453:51-55.
1157 Lammermann, T., and M. Sixt. 2009. Mechanical modes of 'amoeboid' cell migration. *Curr Opin*
1158 *Cell Biol*. 21:636-644.
1159 Lee, B., and D. Lee. 2009. Protein comparison at the domain architecture level. *BMC*
1160 *Bioinformatics*. 10 Suppl 15:S5.
1161 Liu, Y.J., M. Le Berre, F. Lautenschlaeger, P. Maiuri, A. Callan-Jones, M. Heuze, T. Takaki, R.
1162 Voituriez, and M. Piel. 2015. Confinement and low adhesion induce fast amoeboid
1163 migration of slow mesenchymal cells. *Cell*. 160:659-672.
1164 Lo, S.H. 2006. Focal adhesions: what's new inside. *Dev Biol*. 294:280-291.
1165 Lock, J.G., B. Wehrle-Haller, and S. Stromblad. 2008. Cell-matrix adhesion complexes: master
1166 control machinery of cell migration. *Semin Cancer Biol*. 18:65-76.
1167 Lopez-Colome, A.M., I. Lee-Rivera, R. Benavides-Hidalgo, and E. Lopez. 2017. Paxillin: a
1168 crossroad in pathological cell migration. *J Hematol Oncol*. 10:50.
1169 Loveless, T., H. Qadota, G.M. Benian, and J. Hardin. 2017. Caenorhabditis elegans SORB-1
1170 localizes to integrin adhesion sites and is required for organization of sarcomeres and
1171 mitochondria in myocytes. *Mol Biol Cell*. 28:3621-3633.

1172 Martin, F.J., M.R. Amode, A. Aneja, O. Austine-Orimoloye, A.G. Azov, I. Barnes, A. Becker, R.
1173 Bennett, A. Berry, J. Bhai, S.K. Bhurji, A. Bignell, S. Boddu, P.R. Branco Lins, L. Brooks,
1174 S.B. Ramaraju, M. Charkhchi, A. Cockburn, L. Da Rin Fiorretto, C. Davidson, K. Dodiya, S.
1175 Donaldson, B. El Houdaigui, T. El Naboulsi, R. Fatima, C.G. Giron, T. Genez, G.S.
1176 Ghattaoraya, J.G. Martinez, C. Guijarro, M. Hardy, Z. Hollis, T. Hourlier, T. Hunt, M. Kay,
1177 V. Kaykala, T. Le, D. Lemos, D. Marques-Coelho, J.C. Marugan, G.A. Merino, L.P.
1178 Mirabueno, A. Mushtaq, S.N. Hossain, D.N. Ogeh, M.P. Sakthivel, A. Parker, M. Perry, I.
1179 Pilizota, I. Prosovetskaia, J.G. Perez-Silva, A.I.A. Salam, N. Saraiva-Agostinho, H.
1180 Schuilenburg, D. Sheppard, S. Sinha, B. Sipos, W. Stark, E. Steed, R. Sukumaran, D.
1181 Sumathipala, M.M. Suner, L. Surapaneni, K. Sutinen, M. Szpak, F.F. Tricomi, D. Urbina-
1182 Gomez, A. Veidenberg, T.A. Walsh, B. Walts, E. Wass, N. Willhoft, J. Allen, J. Alvarez-
1183 Jarreta, M. Chakiachvili, B. Flint, S. Giorgetti, L. Haggerty, G.R. Ilsley, J.E. Loveland, B.
1184 Moore, J.M. Mudge, J. Tate, D. Thybert, S.J. Trevanion, A. Winterbottom, A. Frankish,
1185 S.E. Hunt, M. Ruffier, F. Cunningham, S. Dyer, R.D. Finn, K.L. Howe, P.W. Harrison, A.D.
1186 Yates, and P. Flicek. 2023. Ensembl 2023. *Nucleic Acids Res*. 51:D933-D941.
1187 McGinnis, S., and T.L. Madden. 2004. BLAST: at the core of a powerful and diverse set of
1188 sequence analysis tools. *Nucleic Acids Res*. 32:W20-25.
1189 Meng, E.C., T.D. Goddard, E.F. Pettersen, G.S. Couch, Z.J. Pearson, J.H. Morris, and T.E. Ferrin.
1190 2023. UCSF ChimeraX: Tools for structure building and analysis. *Protein Sci*. 32:e4792.
1191 Merino-Casallo, F., M.J. Gomez-Benito, S. Hervas-Raluy, and J.M. Garcia-Aznar. 2022.
1192 Unravelling cell migration: defining movement from the cell surface. *Cell Adh Migr*.
1193 16:25-64.
1194 Mijanovic, L., and I. Weber. 2022. Adhesion of Dictyostelium Amoebae to Surfaces: A Brief
1195 History of Attachments. *Front Cell Dev Biol*. 10:910736.
1196 Mitra, S.K., D.A. Hanson, and D.D. Schlaepfer. 2005. Focal adhesion kinase: in command and
1197 control of cell motility. *Nat Rev Mol Cell Biol*. 6:56-68.
1198 Nagasaki, A., M. Kanada, and T.Q. Uyeda. 2009. Cell adhesion molecules regulate contractile
1199 ring-independent cytokinesis in Dictyostelium discoideum. *Cell Res*. 19:236-246.
1200 Niewohner, J., I. Weber, M. Maniak, A. Muller-Taubenberger, and G. Gerisch. 1997. Talin-null
1201 cells of Dictyostelium are strongly defective in adhesion to particle and substrate
1202 surfaces and slightly impaired in cytokinesis. *J Cell Biol*. 138:349-361.
1203 Nordberg, H., M. Cantor, S. Dusheyko, S. Hua, A. Poliakov, I. Shabalov, T. Smirnova, I.V.
1204 Grigoriev, and I. Dubchak. 2014. The genome portal of the Department of Energy Joint
1205 Genome Institute: 2014 updates. *Nucleic Acids Res*. 42:D26-31.
1206 Oakes, P.W., Y. Beckham, J. Stricker, and M.L. Gardel. 2012. Tension is required but not
1207 sufficient for focal adhesion maturation without a stress fiber template. *J Cell Biol*.
1208 196:363-374.
1209 Oakes, P.W., and M.L. Gardel. 2014. Stressing the limits of focal adhesion mechanosensitivity.
1210 *Curr Opin Cell Biol*. 30:68-73.
1211 Oakes, P.W., D.C. Patel, N.A. Morin, D.P. Zitterbart, B. Fabry, J.S. Reichner, and J.X. Tang. 2009.
1212 Neutrophil morphology and migration are affected by substrate elasticity. *Blood*.
1213 114:1387-1395.
1214 Overstreet, M.G., A. Gaylo, B.R. Angermann, A. Hughson, Y.M. Hyun, K. Lambert, M. Acharya,
1215 A.C. Billroth-Maclurg, A.F. Rosenberg, D.J. Topham, H. Yagita, M. Kim, A. Lacy-Hulbert,

1216 M. Meier-Schellersheim, and D.J. Fowell. 2013. Inflammation-induced interstitial
1217 migration of effector CD4(+) T cells is dependent on integrin alphaV. *Nat Immunol*.
1218 14:949-958.
1219 Paluch, E.K., I.M. Aspalter, and M. Sixt. 2016. Focal Adhesion-Independent Cell Migration. *Annu*
1220 *Rev Cell Dev Biol*. 32:469-490.
1221 Pankova, K., D. Rosel, M. Novotny, and J. Brabek. 2010. The molecular mechanisms of transition
1222 between mesenchymal and amoeboid invasiveness in tumor cells. *Cell Mol Life Sci*.
1223 67:63-71.
1224 Parra-Acero, H., M. Harcet, N. Sanchez-Pons, E. Casacuberta, N.H. Brown, O. Dudin, and I. Ruiz-
1225 Trillo. 2020. Integrin-Mediated Adhesion in the Unicellular Holozoan Capsaspora
1226 owczarzaki. *Curr Biol*. 30:4270-4275 e4274.
1227 Parsons, J.T., A.R. Horwitz, and M.A. Schwartz. 2010. Cell adhesion: integrating cytoskeletal
1228 dynamics and cellular tension. *Nat Rev Mol Cell Biol*. 11:633-643.
1229 Patel, H., I. Konig, M. Tsujioka, M.C. Frame, K.I. Anderson, and V.G. Brunton. 2008. The multi-
1230 FERM-domain-containing protein FrmA is required for turnover of paxillin-adhesion sites
1231 during cell migration of Dictyostelium. *J Cell Sci*. 121:1159-1164.
1232 Pawluchin, A., and M. Galic. 2022. Moving through a changing world: Single cell migration in 2D
1233 vs. 3D. *Front Cell Dev Biol*. 10:1080995.
1234 Paysan-Lafosse, T., M. Blum, S. Chuguransky, T. Grego, B.L. Pinto, G.A. Salazar, M.L. Bileschi, P.
1235 Bork, A. Bridge, L. Colwell, J. Gough, D.H. Haft, I. Letunic, A. Marchler-Bauer, H. Mi, D.A.
1236 Natale, C.A. Orengo, A.P. Pandurangan, C. Rivoire, C.J.A. Sigrist, I. Sillitoe, N. Thanki, P.D.
1237 Thomas, S.C.E. Tosatto, C.H. Wu, and A. Bateman. 2023. InterPro in 2022. *Nucleic Acids*
1238 *Res*. 51:D418-D427.
1239 Petrie, R.J., and K.M. Yamada. 2016. Multiple mechanisms of 3D migration: the origins of
1240 plasticity. *Curr Opin Cell Biol*. 42:7-12.
1241 Pinner, S.E., and E. Sahai. 2009. Integrin-independent movement of immune cells. *F1000 Biol*
1242 *Rep*. 1:67.
1243 Plak, K., H. Pots, P.J. Van Haastert, and A. Kortholt. 2016. Direct Interaction between TalinB and
1244 Rap1 is necessary for adhesion of Dictyostelium cells. *BMC Cell Biol*. 17:1.
1245 Potter, S.C., A. Luciani, S.R. Eddy, Y. Park, R. Lopez, and R.D. Finn. 2018. HMMER web server:
1246 2018 update. *Nucleic Acids Res*. 46:W200-W204.
1247 Pribic, J., R. Garcia, M. Kong, and D. Brazill. 2011. Paxillin and phospholipase D interact to
1248 regulate actin-based processes in Dictyostelium discoideum. *Eukaryot Cell*. 10:977-984.
1249 Richardson, L., B. Allen, G. Baldi, M. Beracochea, M.L. Bileschi, T. Burdett, J. Burgin, J. Caballero-
1250 Perez, G. Cochrane, L.J. Colwell, T. Curtis, A. Escobar-Zepeda, T.A. Gurbich, V. Kale, A.
1251 Korobeynikov, S. Raj, A.B. Rogers, E. Sakharova, S. Sanchez, D.J. Wilkinson, and R.D. Finn.
1252 2023. MGnify: the microbiome sequence data analysis resource in 2023. *Nucleic Acids*
1253 *Res*. 51:D753-D759.
1254 Rodriguez-Hernandez, I., G. Cantelli, F. Bruce, and V. Sanz-Moreno. 2016. Rho, ROCK and
1255 actomyosin contractility in metastasis as drug targets. *F1000Res*. 5.
1256 Rokas, A. 2008. The origins of multicellularity and the early history of the genetic toolkit for
1257 animal development. *Annu Rev Genet*. 42:235-251.

1258 Sachdev, S., Y. Bu, and I.H. Gelman. 2009. Paxillin-Y118 phosphorylation contributes to the
1259 control of Src-induced anchorage-independent growth by FAK and adhesion. *BMC*
1260 *Cancer*. 9:12.
1261 Santiago-Medina, M., J.P. Myers, and T.M. Gomez. 2012. Imaging adhesion and signaling
1262 dynamics in Xenopus laevis growth cones. *Dev Neurobiol*. 72:585-599.
1263 Schaller, M.D., and J.T. Parsons. 1995. pp125FAK-dependent tyrosine phosphorylation of
1264 paxillin creates a high-affinity binding site for Crk. *Mol Cell Biol*. 15:2635-2645.
1265 Schaller, M.D., and E.M. Schaefer. 2001. Multiple stimuli induce tyrosine phosphorylation of the
1266 Crk-binding sites of paxillin. *Biochem J*. 360:57-66.
1267 Schick, J., and E. Raz. 2022. Blebs-Formation, Regulation, Positioning, and Role in Amoeboid Cell
1268 Migration. *Front Cell Dev Biol*. 10:926394.
1269 Schindelin, J., I. Arganda-Carreras, E. Frise, V. Kaynig, M. Longair, T. Pietzsch, S. Preibisch, C.
1270 Rueden, S. Saalfeld, B. Schmid, J.Y. Tinevez, D.J. White, V. Hartenstein, K. Eliceiri, P.
1271 Tomancak, and A. Cardona. 2012. Fiji: an open-source platform for biological-image
1272 analysis. *Nat Methods*. 9:676-682.
1273 Sebe-Pedros, A., A.J. Roger, F.B. Lang, N. King, and I. Ruiz-Trillo. 2010. Ancient origin of the
1274 integrin-mediated adhesion and signaling machinery. *Proc Natl Acad Sci U S A*.
1275 107:10142-10147.
1276 Shin, M.E., Y. He, D. Li, S. Na, F. Chowdhury, Y.C. Poh, O. Collin, P. Su, P. de Lanerolle, M.A.
1277 Schwartz, N. Wang, and F. Wang. 2010. Spatiotemporal organization, regulation, and
1278 functions of tractions during neutrophil chemotaxis. *Blood*. 116:3297-3310.
1279 Singiser, R.H., and R.O. McCann. 2006. Evidence that talin alternative splice variants from Ciona
1280 intestinalis have different roles in cell adhesion. *BMC Cell Biol*. 7:40.
1281 Smith, L.A., H. Aranda-Espinoza, J.B. Haun, M. Dembo, and D.A. Hammer. 2007. Neutrophil
1282 traction stresses are concentrated in the uropod during migration. *Biophys J*. 92:L58-60.
1283 Stubb, A., C. Guzman, E. Narva, J. Aaron, T.L. Chew, M. Saari, M. Miihkinen, G. Jacquemet, and J.
1284 Ivaska. 2019. Superresolution architecture of cornerstone focal adhesions in human
1285 pluripotent stem cells. *Nat Commun*. 10:4756.
1286 Sysko, L.R., and M.A. Davis. 2010. From image to data using common image-processing
1287 techniques. *Curr Protoc Cytom*. Chapter 12:Unit 12 21.
1288 Tavares, P., M.C. Rigothier, H. Khun, P. Roux, M. Huerre, and N. Guillen. 2005. Roles of cell
1289 adhesion and cytoskeleton activity in Entamoeba histolytica pathogenesis: a delicate
1290 balance. *Infect Immun*. 73:1771-1778.
1291 Te Boekhorst, V., L. Preziosi, and P. Friedl. 2016. Plasticity of Cell Migration In Vivo and In Silico.
1292 *Annu Rev Cell Dev Biol*. 32:491-526.
1293 Trepat, X., Z. Chen, and K. Jacobson. 2012. Cell migration. *Compr Physiol*. 2:2369-2392.
1294 Tsujioka, M., K. Yoshida, and K. Inouye. 2004. Talin B is required for force transmission in
1295 morphogenesis of Dictyostelium. *EMBO J*. 23:2216-2225.
1296 Tsujioka, M., K. Yoshida, A. Nagasaki, S. Yonemura, A. Muller-Taubenberger, and T.Q. Uyeda.
1297 2008. Overlapping functions of the two talin homologues in Dictyostelium. *Eukaryot*
1298 *Cell*. 7:906-916.
1299 Turner, C.E., J.R. Glenney, Jr., and K. Burridge. 1990. Paxillin: a new vinculin-binding protein
1300 present in focal adhesions. *J Cell Biol*. 111:1059-1068.

1301 Uchida, K.S., and S. Yumura. 2004. Dynamics of novel feet of Dictyostelium cells during
1302 migration. *J Cell Sci*. 117:1443-1455.
1303 van Kempen, M., S.S. Kim, C. Tumescheit, M. Mirdita, J. Lee, C.L.M. Gilchrist, J. Soding, and M.
1304 Steinegger. 2023. Fast and accurate protein structure search with Foldseek. *Nat*
1305 *Biotechnol*.
1306 Varadi, M., S. Anyango, M. Deshpande, S. Nair, C. Natassia, G. Yordanova, D. Yuan, O. Stroe, G.
1307 Wood, A. Laydon, A. Zidek, T. Green, K. Tunyasuvunakool, S. Petersen, J. Jumper, E.
1308 Clancy, R. Green, A. Vora, M. Lutfi, M. Figurnov, A. Cowie, N. Hobbs, P. Kohli, G.
1309 Kleywegt, E. Birney, D. Hassabis, and S. Velankar. 2022. AlphaFold Protein Structure
1310 Database: massively expanding the structural coverage of protein-sequence space with
1311 high-accuracy models. *Nucleic Acids Res*. 50:D439-D444.
1312 Velle, K.B., and L.K. Fritz-Laylin. 2019. Diversity and evolution of actin-dependent phenotypes.
1313 *Curr Opin Genet Dev*. 58-59:40-48.
1314 Velle, K.B., and L.K. Fritz-Laylin. 2020. Conserved actin machinery drives microtubule-
1315 independent motility and phagocytosis in Naegleria. *J Cell Biol*. 219.
1316 Xue, Q., S.R.S. Varady, T.Q.A. Waddell, M.R. Roman, J. Carrington, and M. Roh-Johnson. 2023.
1317 Lack of Paxillin phosphorylation promotes single-cell migration in vivo. *J Cell Biol*. 222.
1318 Yamada, K.M., and M. Sixt. 2019. Mechanisms of 3D cell migration. *Nat Rev Mol Cell Biol*.
1319 20:738-752.
1320 Zhang, W., C.H. Lu, M.L. Nakamoto, C.T. Tsai, A.R. Roy, C.E. Lee, Y. Yang, Z. Jahed, X. Li, and B.
1321 Cui. 2023. Curved adhesions mediate cell attachment to soft matrix fibres in three
1322 dimensions. *Nat Cell Biol*. 25:1453-1464.
1323 Zhao, A.J., J. Montes-Laing, W.M.G. Perry, M. Shiratori, E. Merfeld, S.L. Rogers, and D.A.
1324 Applewhite. 2022. The Drosophila spectraplakin Short stop regulates focal adhesion
1325 dynamics by cross-linking microtubules and actin. *Mol Biol Cell*. 33:ar19.
1326
1327